Department of Environment, Land and Infrastructure Engineering

Master of Science in Petroleum and Mining Engineering

A.Y. 2022/2023

Master Thesis in Petroleum Engineering

Capillary Desaturation Curves for CO_2-Water systems

Supervisor:

Prof. Francesca VERGA

Dott. Alessandro SURIANO

Candidate:

Pasquale CAPOZZOLI

301835

22 November 2023

ABSTRACT

CO_2 capture and storage is one of the most important ways to reduce greenhouse emissions and thus reduce the increase of the world average temperature. Deep saline aquifers are suitable geological formations for CO_2 underground storage in a permanent and safe way. Among the different trapping mechanisms, residual CO_2 trapping indicates the trapping of the injected carbon dioxide inside the rock pores thanks to capillary forces. Residual CO_2 saturation when the CO_2 plume migrates through the aquifer cannot be predicted and must be assessed experimentally.

The Capillary Desaturation Curve obtained from laboratory data is the most used plot to evaluate the residual CO_2 saturation as a function of the Capillary number, expressing the ratio of viscous to capillary forces. The Capillary Desaturation Curves can also be plotted as a function of the Trapping number, which includes both the capillary number and the gravitational effect through the Bond number.

In this study, the assessment of the residual CO_2 saturation was performed for two rock samples, a sandstone and a carbonate, through core flooding experiments with a Relative Permeability System.

Firstly, CO_2 was injected to evaluate the residual water saturation; then, water was injected at increasing rates until quasi-steady state was reached.

The residual CO_2 saturation was calculated for each step and plotted as a function of the Capillary number. Two different definitions of the Capillary number were considered and used to calculate the Trapping number and plot the Capillary Desaturation Curve.

Results confirmed that the residual CO_2 saturation depends on the rock absolute permeability but also on the injection rate. As expected, when the injection rates are high, gravitational effects become negligible. The effects of solubility, salinity and contact angle were not assessed in this work because the experiments are extremely long (in the order of weeks), so further investigations would be needed to assess the impact of these parameters on the Critical Capillary number.

ACKNOWLEDGEMENTS

I would sincerely like to thank my supervisor Professor Francesca Verga for the availability and the opportunity to be part of the research team during the last months and my co-supervisor Alessandro Suriano for the daily availability and the constant help during the whole project.

INDEX

LIST OF FIGURES

LIST OF TABLES

1. INTRODUCTION

1.1. CCS IN THE WORLD

Since prehistory, resources have defined the eras of civilization, with the evolution of technology the world has used new sources of energy and, consequently, society has seen several revolutions that have changed human life on our planet.

Since the industrial revolution, fossil fuels have led to the creation of the occidental socio-economic system and have shaped modern society. Their use was the first step of the world's evolution, and, without the eras of coal and oil, the development of society would have been much different.

However, fossil fuels exploitation is one of the causes of air pollution, its combustion emits greenhouse gases. This is one of the factors that leads to the average world's temperature increase. Today, we use fossil fuels (coal, oil, and gas) to satisfy society's needs. Due to the continuous growth of Earth's population and the development of society's industrialization, the energy demand will increase and, greenhouse gas emissions will rise. GHGs in Earth's atmosphere trap heat, for this reason, an excess CO_2 traps more heat and causes it to become warmer [1].

In the last decades, the scientific community has been dealing with the energy transition challenge to start counteracting the climate change effects. The UNFCC (United Nations Framework Convention on Climate Change) was born in 1992, ratified by 197 countries, to establish an international treaty to combat dangerous human interference with the climate system [2]. The Conference Of Parties (COP) has resulted in the Kyoto Protocol (COP3 1997) and the Paris Agreement (COP21 2015), the basis of climate law [3]. The last one, COP27, took place in Egypt (2023) and had two important outcomes: the creation of a loss and damage fund to compensate economically the vulnerable countries, damaged by climate events, and the confirmation of a 1.5°C limit to the global temperature increase [4].

Europe is taking a leading role in fighting climate change, with the goal to achieve net-zero greenhouse gas (GHG) emissions by 2050. The European Commission sets the European Green Deal [5] to define a new growth strategy to lead toward a more sustainable path. The 27 EU Member States pledged to reduce emissions by at least 55% by 2030, compared to 1990 levels [6].

The way to achieve this goal is defined in the European Strategic Energy Technology Plan (SET-Plan) [7], where ten priority areas are defined, covering a wide range of technologies including wind, solar, geothermal, renewable energy, heating and cooling, biofuels, and Carbon Capture Utilisation and Storage (CCUS).

The main strategy is a complete switch from oil and coal to natural gas supported by renewable energy and to reduce the emissions thanks to CO_2 Capture and Storage (CCS) [1]. Natural gas is considered the environmentally acceptable fossil fuel, because of its combustion releases lower greenhouse emissions; it is necessary to support the energy demand during the transition.

CCUS is a mitigation measure that prevents large amounts of carbon dioxide from emission sources, such as energy-intensive industries and power plants, from being released into the atmosphere [8]. Technology involves capturing CO_2, compressing it for transportation and selling it to users such as enhanced oil recovery or other industrial processes or injecting it as a supercritical fluid into a deep rock formation.

This thesis is linked to the storage of CO_2. Understanding the behaviour of CO_2 underground storage is fundamental to design in the best way the plant and the injection facilities, reduce the risk of geomechanics failure and ensure correct storage.

All the indications about the role of CCUS and necessary actions are reported in the CCUS Roadmap to 2023 [9]. According to this document, the scale-up of CCUS supports the EU transition, preserves jobs, stimulates economic growth, and diversifies the supply chain into new industries.

CCUS is aligned with the Sustainable Development Goals [10]: n. 3 “Good health and well-being”, n. 7 “Affordable and clean energy”, n. 8 “Decent work and economic growth”, n. 9 “Industry, innovation and infrastructure”, n. 12 “Responsible consumption and production”.

The Net Zero Roadmap: A Global Pathway to Keep the 1.5°C Goal in Reach published in 2023 [8], asserts that CCUS can contribute by 8% of cumulative emissions reductions. In Figure 1, the past trend and the forecast of capture capacity in the world, if the current European policy is applied, can be seen.

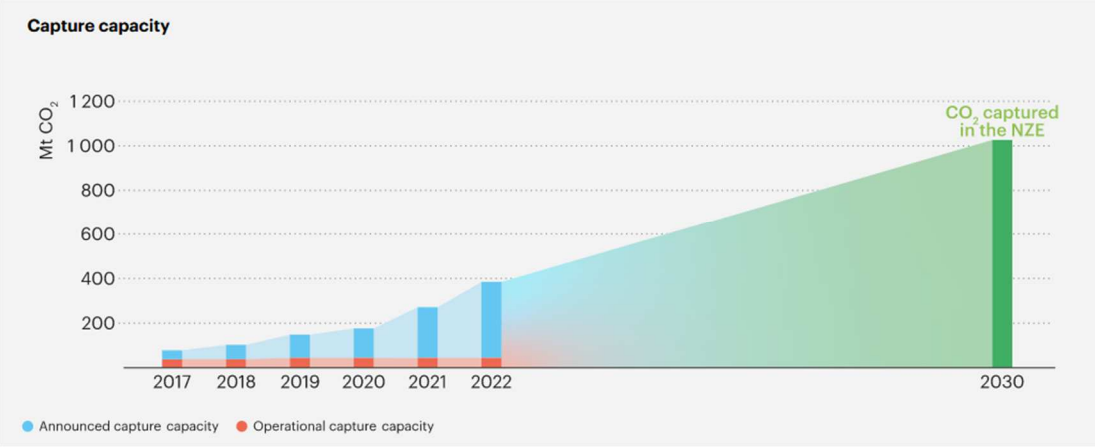

Figure 1 - Trend of capture capacity [8].

The Global CCS Institute, as shown in Figure 2, reports that the number of CCS projects active in the whole stages is 257 with a total capture capacity of 257 Mtpa [11].

Q2 2023

2023	OPERATIONAL	IN CONSTRUCTION	ADVANCED DEVELOPMENT	EARLY DEVELOPMENT	TOTAL
Number of Facilities	37	20	97	103	257
Capture Capacity	50.6	22.9	85.5	148.8	307.8

Q4 2022 (Global Status Report '22)

2022	OPERATIONAL	IN CONSTRUCTION	ADVANCED DEVELOPMENT	EARLY DEVELOPMENT	SUM
Number of Facilities	30	11	78	75	194
Capture Capacity	42.5	9.6	97.6	91.8	241.6

Figure 2 - Current commercial CCS facilities by number and total capacity [11].

The Global Status of CCS 2022 [12] maps the active projects, shown in Figures 3 and 4, and underlines the interest of developed countries in this technology.

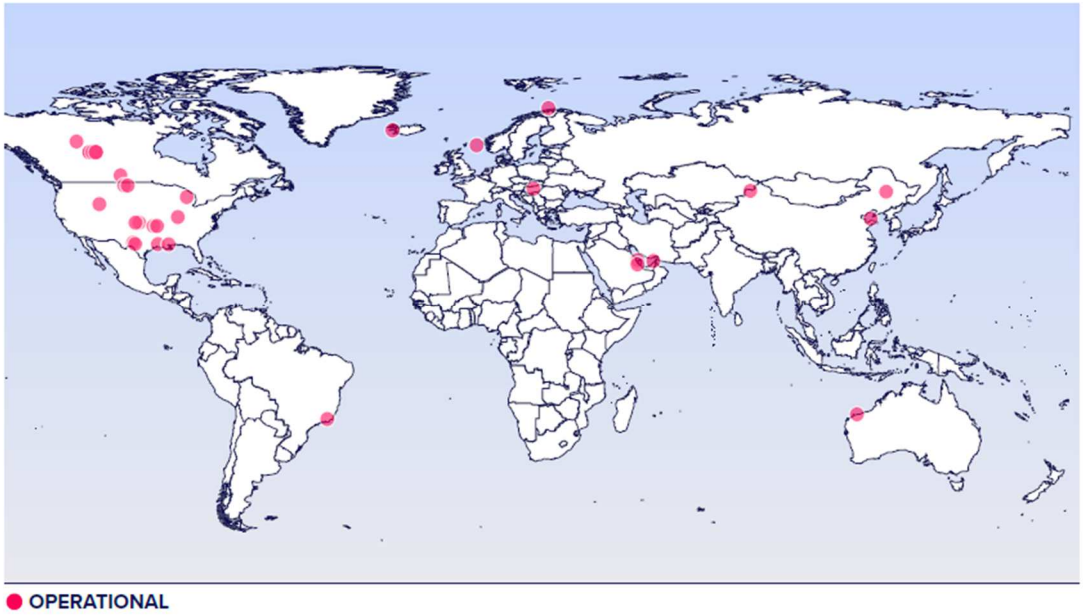

Figure 3 - World map of CCS operational facilities (2022) [12].

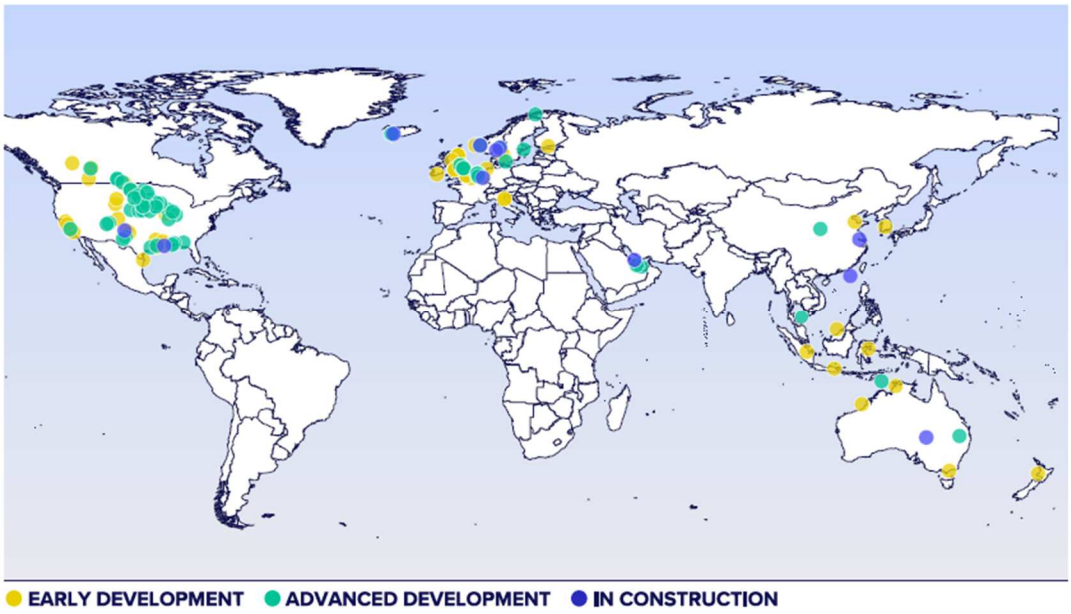

Figure 4 - World map of CCS facilities at various stages of development [12].

1.2. EVOLUTION OF STORAGE

CO_2 storage in deep underground formations can be a safe strategy to store permanently carbon dioxide and reduce its emission in the atmosphere. The geological formations that have the required features for gas storage are depleted oil and gas reservoirs and deep saline aquifers. Also, salt cavities and abandoned mines can be used [13]. The main characteristics are the following ones.

- Injectivity, the capability of injecting CO_2 at the designed rate during a defined period (related to the emission rate of the source associated with the storage site).
- Storage capacity, the amount of CO_2 that can be safely injected.
- Containment, the capability of keeping the injected CO_2 in the geologic formation targeted for storage during a long period of time, without impairing health, safety, or the environment.

Historically, CO_2 has been used in the Oil & Gas industry to enhance oil recovery from reservoirs; today, the most important type of storage is the injection in deep saline formations, as shown in Figure 5. For CO_2 storage, other important factors that must be considered are trapping mechanisms and geochemical interaction. When the CO_2 is injected inside the geological formation, it dissolves in water and carbonic acid is formed. This acid reacts with the formation water, it causes a weak acidification and corrosion problems of well completion can occur. CO_2 dissolved reacts also with the formation rock minerals, it enables mineral dissolution that increases permeability and jeopardises the cap rock integrity, and the generation of secondary minerals from salt precipitation that causes a decrease in injectivity.

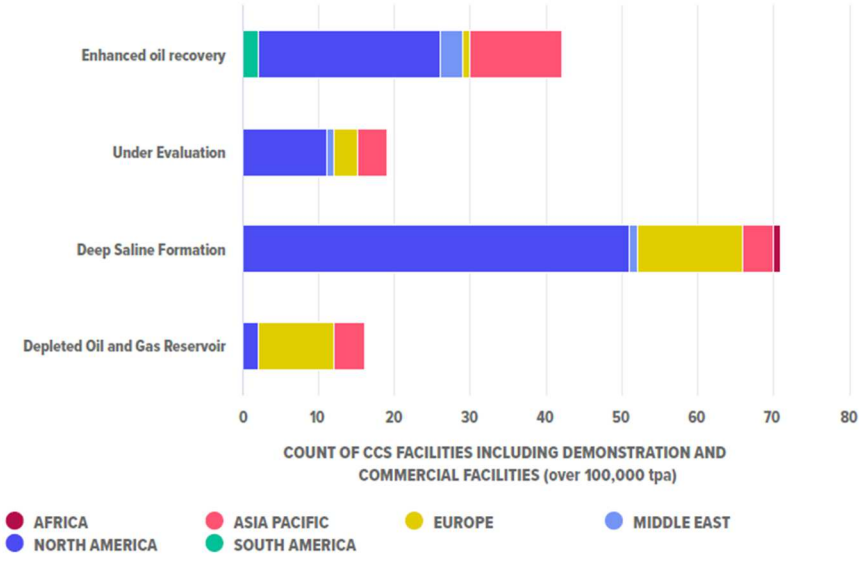

Figure 5 - Count of CCS facilities across storage types and geographies [12].

1.3. CO_2 GEOLOGICAL STORAGE

Understanding the CO_2 behaviour when injected in geological formations is fundamental to assessing the trapping mechanisms, for the evaluation of the storage capacity, the containment, and the geochemical interactions. There are four CO_2 trapping mechanisms, as reported in the Intergovernmental Panel on Climate Change [14] and in the Global Status of CCS 2022 [12].

- Structural and stratigraphic trapping: flowing back is prevented by an impermeable layer; CO_2 rises towards the caprock due to buoyancy forces, when it reaches the top of the formation, vertical flow is stopped and slowly laterally flow occurs (hydrodynamic trapping) [13].
- Residual CO_2 trapping (Capillary trapping): after injection, when CO_2 migrates laterally and upward, water displaces CO_2 in an imbibition-like process; this leads to the drop's disconnection from the plume and the formation of residual trapped CO_2 inside the pores. The study of this thesis is focused on the definition of a Capillary Desaturation Curve for a CO_2-water system, thanks to that, the evaluation of CO_2 residual saturation after the imbibition process with different rates is feasible in sandstone and carbonate.
- Solubility trapping: dissolution and hydration of CO_2 in the water to form carbonic acid, it forms a weak acid, and the evaluation of the solubility is still very difficult.
- Mineral trapping: interaction of dissolved CO_2, water and rock enables mineral dissolution and generation of secondary minerals from precipitation.

As shown in Figure 6, the relative contribution of each trapping mechanism changes with time and with the CO_2 plume's evolution. Initially, in the first decades, the most important process is the physical trapping (structural/stratigraphic/hydrodynamic and residual CO_2 trapping). After hundreds of years, the importance of physical trapping decreases and the impact of geochemical one starts to increase (solubility and mineral trapping). The storage security increases over time.

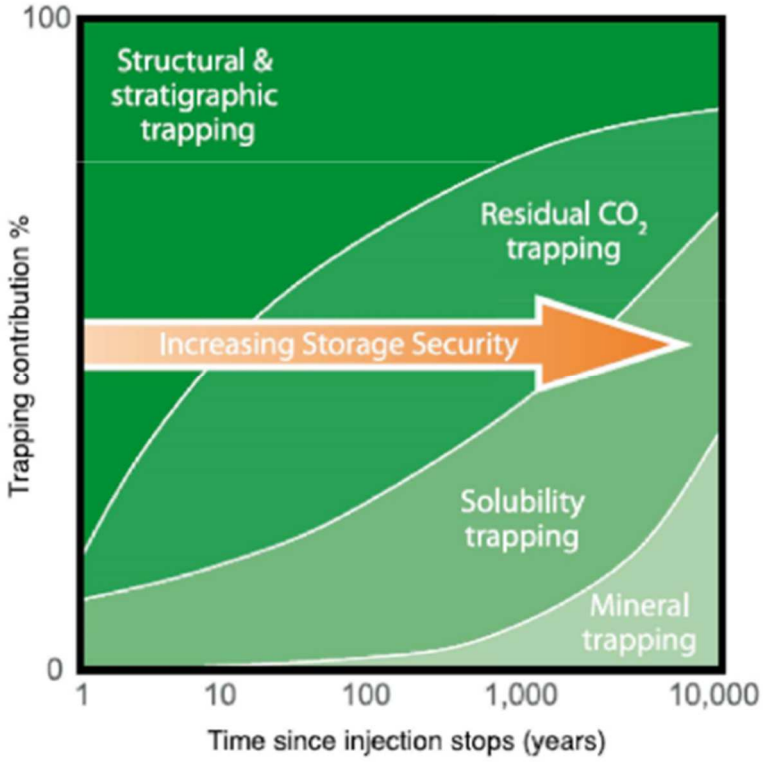

Figure 6 - Time evolution of trapping mechanisms [14].

2. LITERATURE REVIEW

The scope of this study is to better characterize capillary trapping during carbon dioxide injection in a deep saline aquifer, this mechanism represents an effective and secure phenomenon to immobilize the injected CO_2 inside the rock pores [15]. Capillary trapping plays a fundamental role in CO_2 storage. The goal is to maximise the trapped carbon dioxide during the CO_2 injection. One possible strategy can be an additional water injection to push the CO_2 plume and enhance the imbibition process [16].

Capillary trapping is the disconnection of the CO_2 phase into an immobile (trapped) fraction. Carbon dioxide is the non-wetting fluid and water is the wetting fluid, the system is water wet. During the CO_2 injection, the formation water is displaced in a drainage process (when the non-wetting fluid displaces the wetting fluid), and a plume is formed. Due to the immiscibility and the density contrast, the buoyant CO_2 migrates laterally and upward, and water displaces carbon dioxide in an imbibition-like process (when the wetting fluid displaces the non-wetting fluid). This leads to the disconnection of the once-continuous plume and a CO_2 fraction is trapped in the pore space [17].

If the CO_2 residual saturation ($S_r^{CO_2}$) is estimated, the capillary trapping capacity (C_{trap}) of a given rock (Φ: porosity) can be determined with Eq. 1.

$$C_{trap} = \Phi \, S_r^{CO_2} \qquad \text{Eq. 1}$$

During imbibition, a fraction of CO_2 is trapped and disconnected in blobs, only by increasing the flow rate we can remobilize these blobs [18]. There are different basic displacement mechanisms, as shown in Figure 7.

- Piston-type motion (Figure 7 a): frontal meniscus is inside the duct. Motion can occur both in the drainage and imbibition process.
- Snap-off (Figure 7 b): frontal meniscus isn't inside the duct, isolated blobs are created, especially in a loop structure. Only in the imbibition process.
- Imbibition 1 (Figure 7 c): only the non-wetting fluid is present in the duct. Only in the imbibition process.
- Imbibition 2 (Figure 7 d): collapse occurs because the non-wetting fluid is in two adjacent ducts. Only in the imbibition process [19].

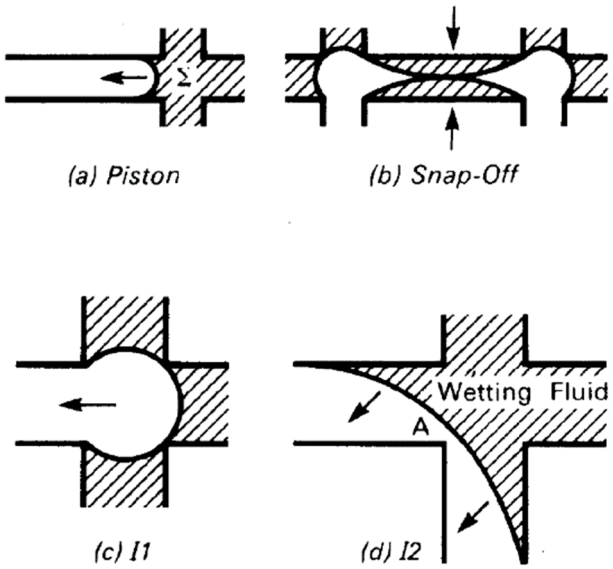

Figure 7 – Representation of basic displacement mechanisms [18].

Processes during carbon dioxide storage are: CO_2 displaces resident brine and relative permeability is high, brine imbibes the plume and a disconnected fluid saturation occurs and the residual immobile CO_2 is trapped within the formation (a sketch of fluid flow during buoyant CO_2 migration in a reservoir is shown in Figure 8) [20].

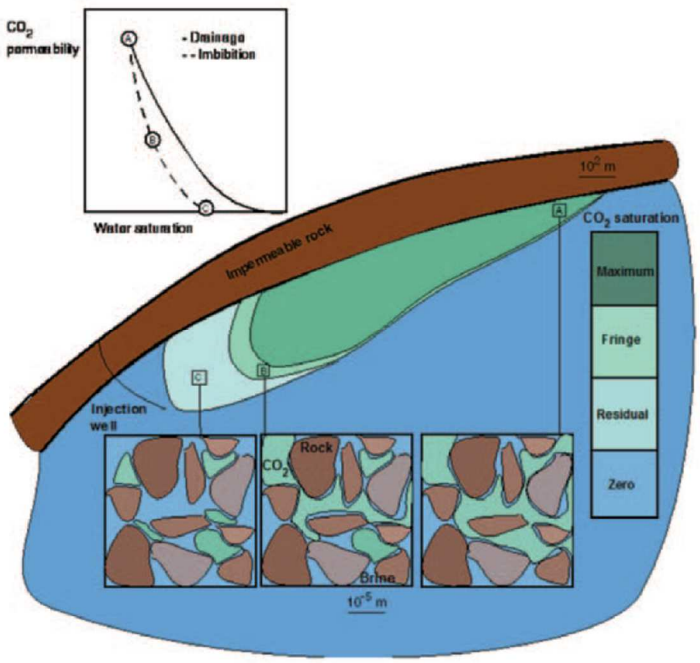

Figure 8 - Flow processes [20].

2.1. CAPILLARY NUMBER

Capillary number is essential to designing a desaturation experiment and interpreting in a proper way the results. It is defined as the ratio between viscous and interfacial tension forces. Quantifying the relationship between viscous and capillary forces is very controversial, finding a suitable definition is necessary to estimate the correct Capillary Desaturation Curve [21].

The capillary force is responsible for the CO_2 trapping, in classic definition larger Capillary number leads larger displacement of the non-wetting fluid. In EOR application this effect is a problem that decreases the recovery factor, the amount of oil or gas produced. In CO_2 storage application this trapping mechanism can be useful to safely store a certain capacity of carbon dioxide.

The most used formulation for the Capillary number is Eq. 2 (v: velocity, μ: viscosity, σ: interfacial tension) [22]–[27].

$$N_{cap} = \frac{viscous\ force}{intefacial\ force} = \frac{v\,\mu}{\sigma} \qquad \text{Eq. 2}$$

Ideally, using Eq. 2, a Capillary number equal to one represents the transition from capillary-dominated to viscous-dominated flow; however, when the forces are equal, the classic Capillary number is $2.2*10^{-3}$. The most important difficulty is the flow characterization [21].

Moore and Slobod in 1955 [28] presented Eq. 3 (v: velocity, μ: viscosity, σ: interfacial tension, θ: contact angle). This formulation can present a problem when $\cos(\theta) = 0$, when the contact angle is almost 90° the expression is not suitable, usually $\cos(\theta)$ is omitted and Eq. 2 is used.

$$N_{cap} = \frac{v\,\mu}{\sigma\cos(\theta)} \qquad \text{Eq. 3}$$

Abrams in 1975 [29] presented Eq. 4 (v: velocity, μ_{water}: water viscosity, μ_{oil}: oil viscosity σ: interfacial tension).

$$N_{cap} = \frac{v\,\mu_{water}}{\sigma}\left(\frac{\mu_{water}}{\mu_{oil}}\right)^{0.4} \qquad \text{Eq. 4}$$

Eq. 4 is the first capillary number definition that incorporates the viscosity ratio [29]. In this study, different sandstone and limestone core flow tests are performed to show the influence of interfacial tension, fluid viscosity and flow velocity. The exponent 0.4 is purely experimental, it is the best value to fit the data, and with respect to Eq. 2 shows a lower scattered in data points. CDCs resulting from this study are plotted in Figure 9. The viscosity ratio is a key factor to include the sweep efficiency in the capillary number.

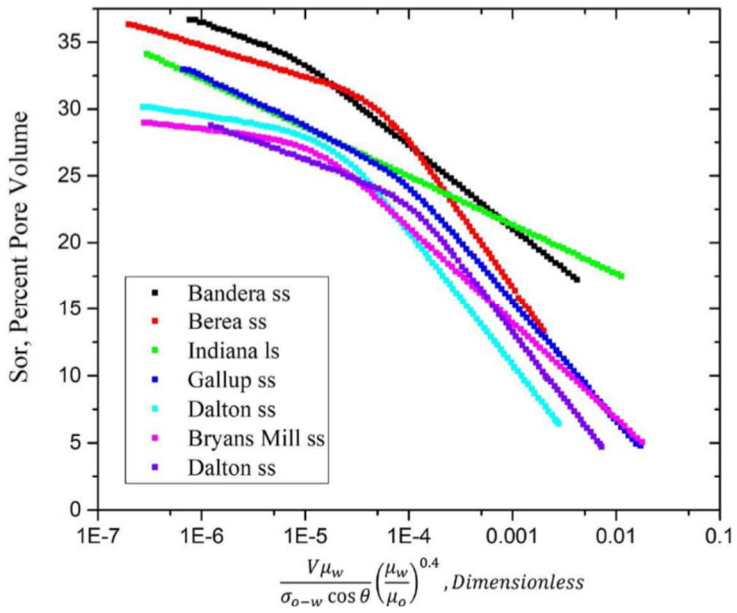

Figure 9 - CDCs for the different tests with Abrams 1975 capillary number [29].

In 2017, Doorwar and Mohanty [30] updated Eq. 4 in Eq, 5, adding the diameter of the core (D) and absolute permeability (k), and changing the viscosity ratio exponent from 0.4 to -2. This equation results in conflict with Eq. 4, and it was introduced as an instability number where not only sweep efficiency but also displacement efficiency is included.

$$N_{cap} = \frac{v\,\mu_{water}}{\sigma}\left(\frac{\mu_{water}}{\mu_{oil}}\right)^{-2}\frac{D^2}{k} \qquad \text{Eq. 5}$$

From the literature, it is appreciated that the Capillary number depends on the length scale. All the involved forces on the pore scale differ from those on the laboratory scale and, from those on the field scale. Due to the scale dependency, understanding the physical behaviour is fundamental to representing in the best possible way the phenomenon. The flow is dominated by capillary force at a small scale; on the other hand, by viscous force at a large scale, as shown in Figure 10.

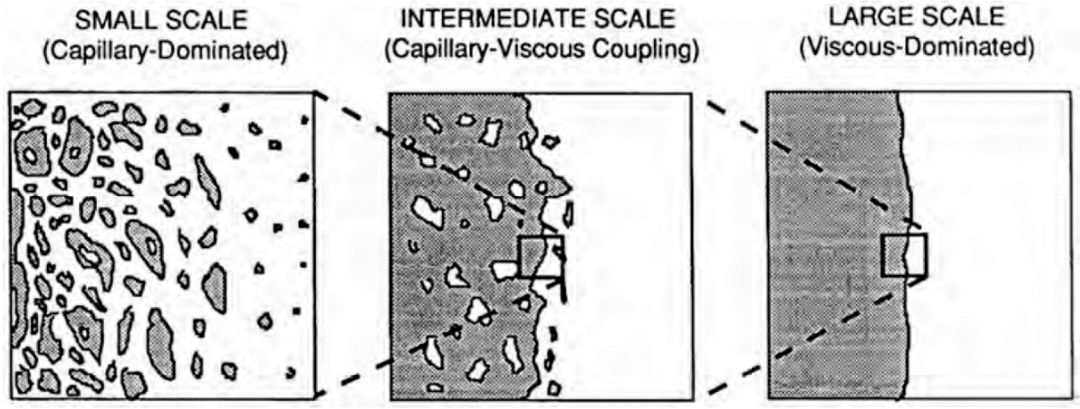

Figure 10 - The scale-dependence of force balance [31]..

At different scales, different characteristic parameters are used, for this reason, the upscaling process is misleading [32], mostly due to the heterogeneity.

Because of this problem, in the literature, a scale-dependence classification for Capillary number is introduced: microscopic scale, mesoscopic scale and macroscopic scale. The use of one or another depends on the engineering goal. When the capillary and viscous forces are both characterized by microscopic parameters the use of a microscopic scale is recommended, if both by macroscopic one macroscopic scale is suggested. If one is microscopic and the other is macroscopic the ratio is called mesoscopic.

- Microscopic Capillary Numbers are calculated from core flooding tests. They can be combined with macroscopic velocity only if the porous media is homogeneous. The sweep efficiency is neglected. The main flow mechanisms are film swelling, cooperate pore filling, snap-off, droplet fragmentation, coalescence and corner flow.
- Mesoscopic Capillary Numbers are modified capillary numbers that contain some microscopic parameters such as velocity and interfacial tension, and some macroscopic parameters as porosity and permeability. They are useful to evaluate the flow transition from microscopic to macroscopic regime. Their value is higher than microscopic ones.
- Macroscopic Capillary Numbers are applied to analyse the dynamic force with macroscopic gravity numbers. They include macroscopic parameters like permeability, porosity and capillary pressure. Viscosity is used and it’s more representative than interfacial tension.

In the last decades, at least 41 different Capillary numbers have been defined. The problem is finding a precise characterization for the viscous and capillary forces. The new Capillary numbers are based on the traditional definition, updated with a scaling group to add the scale dependency. However, the main limit of new Capillary numbers is the proper definition of this scaling number that contains empirical parameters estimated for model or numerical simulation; the estimation of these parameters for a real rock sample is very complex, many additional tests on the plug are required to try to estimate correct values [21].

2.2. TRAPPING NUMBER

Multiphase flow in porous media depends on capillary, viscous and gravitational forces. Capillary number considers only the capillary and viscous forces.

To also consider the gravitational effect a new parameter, called Bond number is used (Eq. 6). The Bond number is defined as the ratio between gravitational and interfacial forces (Δp: pressure drop across core, k: relative permeability, r: distance from axis of rotation to the closest point of the core, w: rate of rotation, σ: interfacial tension) [33].

$$N_{bond} = \frac{\Delta p \; k \; r \; w^2}{\sigma} \qquad \text{Eq. 6}$$

To assess this parameter, a centrifuge test is recommended at rotational speeds high enough to overcome capillary force.

When the test are not performed, an analytical equation is defined to estimate the Bond number of a rock core (Eq. 7 - K: absolute permeability, Δρ: density difference between displacing and displaced phases, g: gravity acceleration) [26].

$$N_{bond} = \frac{\mathrm{K}\,\Delta\rho\; g}{\phi\; \sigma \cos(\theta)} \qquad \text{Eq. 7}$$

The Trapping number combines the effects of capillary and viscous forces (N_{cap}) with the gravitational ones (N_{bond}) considering the inclination of the core sample (θ is the angle from the horizontal level) or anisotropy of the formation [34].

$$N_{trap} = \sqrt{N_{cap}^2 + 2\; N_{cap} N_{bond} \sin(\theta) + N_{bond}^2} \qquad \text{Eq. 8}$$

CDCs can be also plotted as a function of the Trapping number (N_{trap}) to consider also the effect of gravitational force.

2.3. CAPILLARY DESATURATION CURVE

Several laboratory experiments have been conducted in CO_2-water systems with rock samples at reservoir conditions to investigate the displacement between supercritical CO_2 and water, and provide parameters estimations for aquifer storage capacity [35].

The Capillary Desaturation Curve (CDC) represents the relationship between the residual saturation of the non-wetting fluid and the Capillary number or a combination of the Capillary and Trapping numbers. It is one of the most important curves of oil recovery and the fundamental one for the design of new CO_2 storage projects.

Starting from an initial saturation of non-wetting fluid (in this study CO_2), CDC ends at some residual saturation of that fluid, depending on many parameters and conditions related to fluids, rock and injection rate [21].

$$CDC : [0,1]\ x\ \mathbb{R}\ x\ \ldots \rightarrow [0,1]$$
$$\left(S_{CO_2}^{ini}, Ca, \ldots\right) \rightarrow S_{CO_2}^{res} = CDC\ \left(S_{CO_2}^{ini}, Ca, \ldots\right) \qquad \text{Eq. 9}$$

The $S_{CO_2}^{res}$ is the fraction of CO_2 trapped in pore volume after the water imbibition (considering no capillary end effects), for the evaluation of this parameter the literature suggests a combination of different techniques such as corefloods, centrifuge and log-inject-log [23], [36], [37].

Several experiments, using both coreflood and centrifuge techniques, have been conducted on sandstone and carbonate with oil and water, gas and water, and only a few with CO_2 and water.

An important parameter that can be estimated by plotting CDCs is the Critical Capillary number is defined as the inflexion point where the residual saturation starts decreasing.

Classical CDC is defined as a monotonically curve that decreases as the Capillary/Bond/Trapping number increases, with the presence of only one critical capillary number.

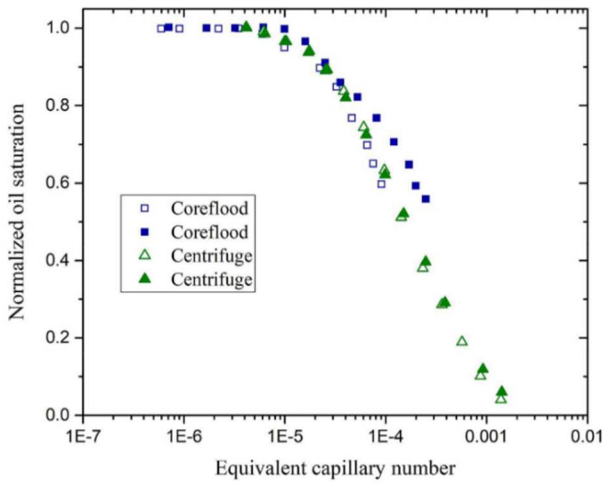

Figure 11 - CDC using coreflood and centrifuge technique [33].

In the study of King et al. [33], a comparison between the two techniques is made, as shown in Figure 11. The result is a similar trend, the two obtained datasets are aligned.

In the study of Lake et al. [27], the dependency of residual saturation for the non-wetting and wetting phase on the capillary number has been observed, as shown in Figure 12.

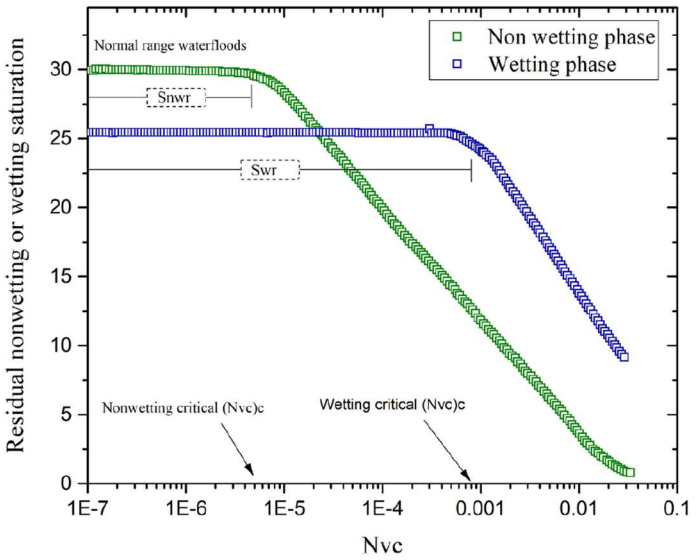

Figure 12 - Schematic diagram for CDC for wetting and non-wetting phases [27].

In the study of Garnes et al. 1990 [38] the effect of the petrophysical properties on CDC is estimated. The critical capillary number decreases if the permeability increases.

Furthermore, the difference between sandstone and carbonate CDC was presented by Tang and Harker 1991 [39]. The CDC of carbonate appears steeper but wider than sandstone rock because of non-uniform pore size distribution, as shown in Figure 13.

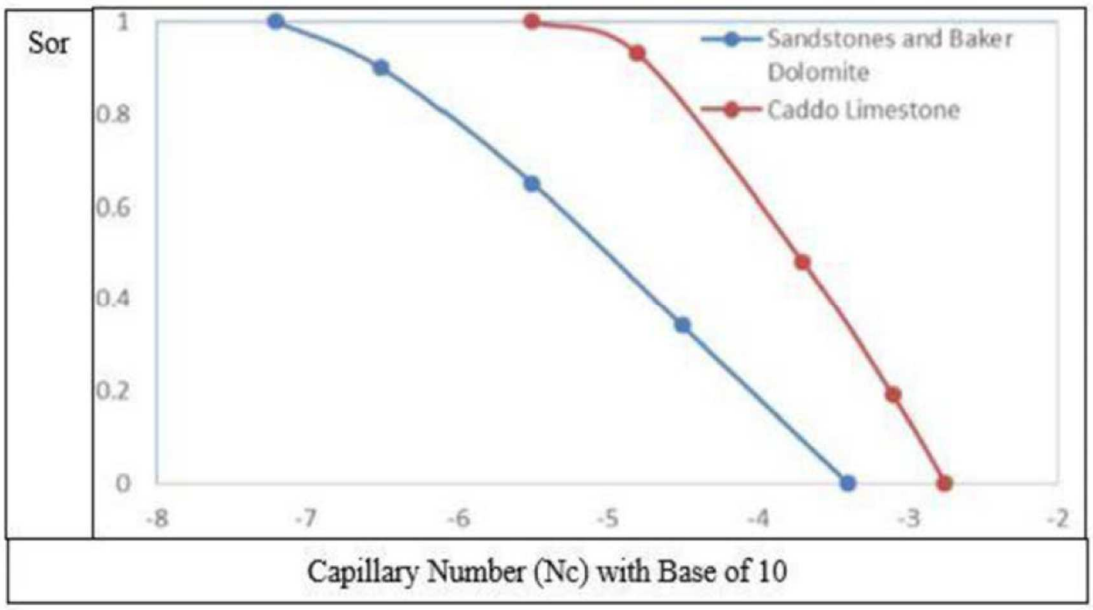

Figure 13 - Comparison of CDC for sandstone and carbonate [39].

New CDCs are defined as a curve in which the residual saturation increases or decreases as the Capillary/Bond/Trapping number increases, due to insufficient sweep efficiency, discontinuous waterflood saturation and not incorporating the viscosity ratio [16]. A second critical capillary number can be defined as the second inflection point, after the first critical capillary number and stabilization saturation start increasing and then decrease again, as shown in Figure 14. The main difference between the classical and new CDCs is in defining a capillary number without including the macroscopic sweep efficiency. The definition of CDC is strictly related to the definition of Capillary number, as shown in the following section, different approaches can lead to very different results.

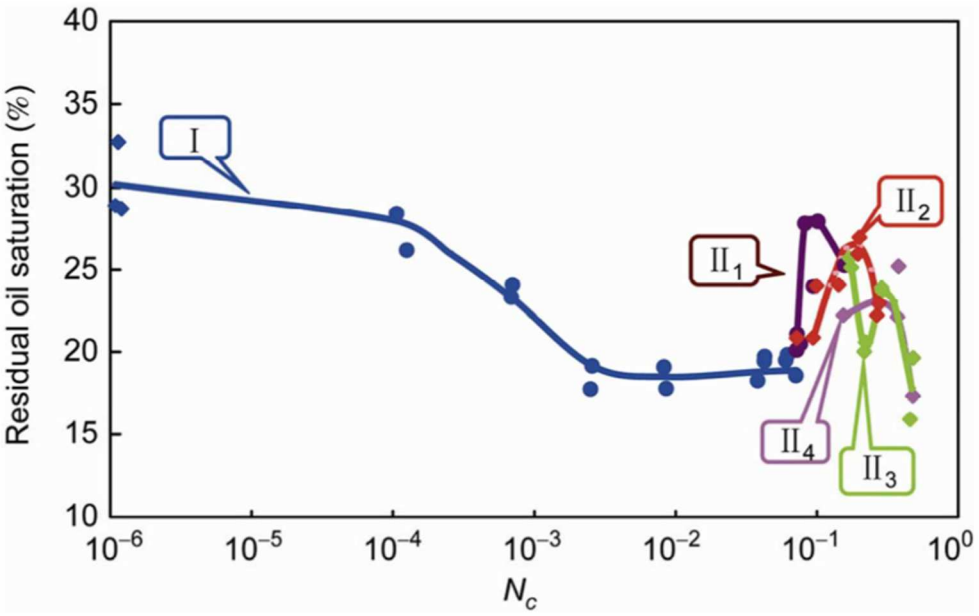

Figure 14 - New CDC [16].

2.4. FACTORS AFFECTING CDC

In the last two decades, several experiments on CO_2-water systems have been performed, due to the increasing interest in CO_2 storage projects [15].

Several impacts are assessed and different recommendations are given for better design of the future tests. A brief review of the known impacts is given to evaluate in the best possible way all the problems that can change the test results.

For a coreflood experiment the equilibration of the phases is fundamental to prevent mass transfer across the phase interface. If the phases are not mutually equilibrated, the saturation changes, and this effect is not caused by capillary forces. In several applications an equilibration reactor is installed [15]. The equipment used for this study does not include this tool, to prevent the mass transfer between CO_2 and water an initial test has been done for several days to stabilize the conditions and eliminate the solubility problem from the system.

The study of Ding et al. 2004 [40] evaluates the critical capillary number for mobilizing gas from water and oil imbibition, to assess the different behaviour. The tests on the water-gas system are run for spontaneous and forced imbibition. For the spontaneous one, the gas saturation decreases rapidly in the first 20 minutes and then slows down. For forced one, the gas saturation remains constant until the flow rate reaches a certain point corresponding to the critical capillary number, as shown in Figure 15. The results show that after shutting off the injection, the gas saturation increases, when the injection is shut off, the pressure on the plug is released and gas bubbles expand displacing water. The water saturation increase is partially due to gas production, also gas compression influence has an impact. From this study it can be concluded that the true gas saturation is affected by gas compressibility and the critical capillary number for gas-water systems is much smaller than for oil-water systems, it is easier to remobilize the trapped gas than the trapped oil. The following tests of Ding et al. 2005 observe that the critical capillary number does not depend on the initial experimental procedure [41], but the residual saturation is lower for connected fluid (connected fluid is more recoverable than the disconnected one) [42].

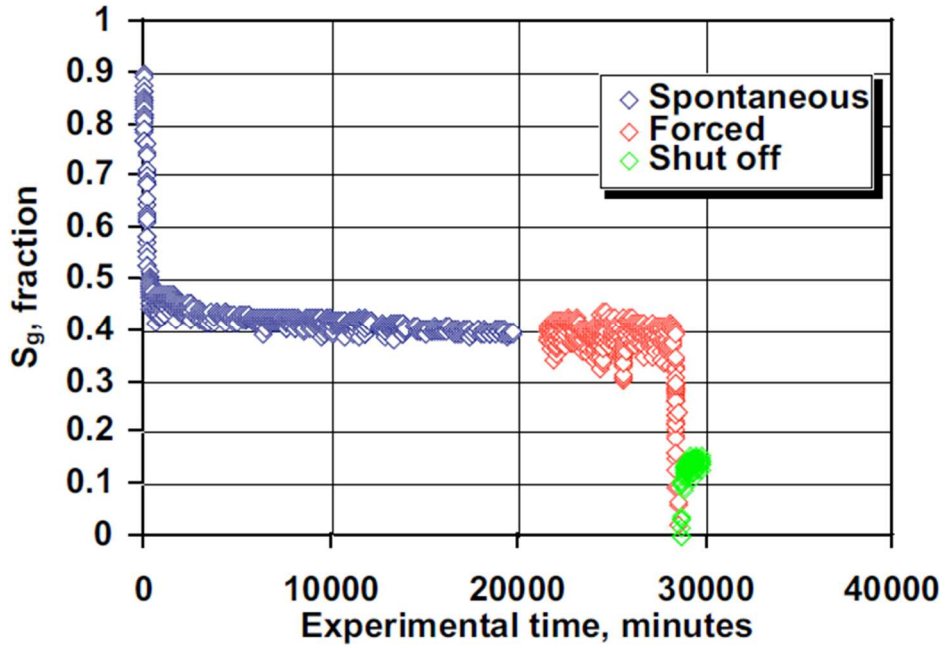

Figure 15 - Gas saturation variation in time in a gas-water system with spontaneous and forced imbibition [40].

The study of Chang et al 2019 analyses the unstable drainage process caused by CO_2 injection in deep aquifers, rescaling the relationship between CO_2 saturation and capillary number by using a complete capillary number that accounts for pore structure [35]. During each drainage experiment, CO_2 is injected at a constant flow rate until the quasi-steady state is reached to have a distribution and saturation stable in time for different micromodels, as shown in Figure 16. Pore geometry has a huge impact on unstable drainage experiments and a complicated complete capillary number can improve the comparison between different models. This study also investigates the effects of capillary on viscous fingering, performing constant-rate and step-rate injection experiments. The step-rate method is less efficient than the constant-rate one, because the saturation at each step is lower than the corresponding for constant-rate (more volume injection is required to reach the quasi-steady state).

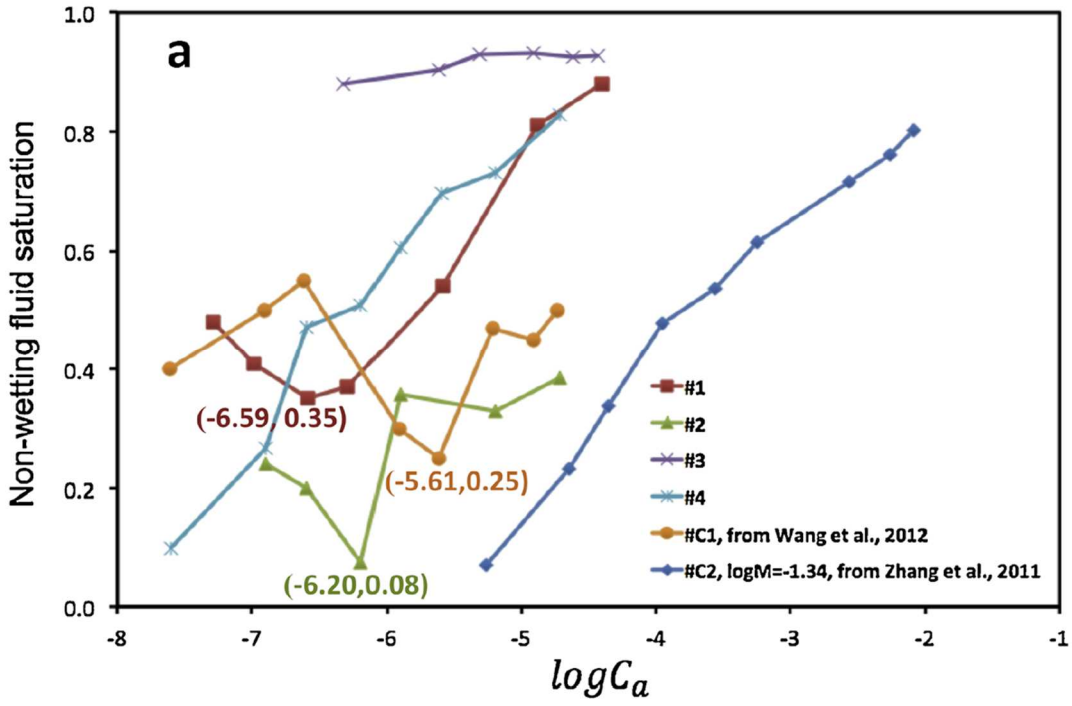

Figure 16 - Non-wetting fluid saturation vs. log (Capillary number) [35] for the drainage experiment conducted in different micromodels and in Wang et al. 2012 [43] and Zhang et al. 2011 [44].

The study of Hilfer et al. 2015 measures the Capillary Desaturation Curve, analysing two different modes. A discontinuous mode desaturation starts from a sample filled with non-wetting fluid and continues with wetting fluid injection in steps, the result is a discontinuous residual fluid inside the pores. A continuous mode desaturation starts with a configuration in which the resident fluid is hydraulically connected to the inlet and outlet; increasing the injection rate, the sample is emptied, refilled, and then injected with a new increased rate. Experiments in continuous are more expensive and difficult than discontinuous ones [45]. The efficiency of displacement depends on the desaturation mode due to the different fluid distribution inside the core [46].

Humphry et al. 2014 found a strong interrelation between wettability, residual oil saturation and, critical capillary and bond number. If the system becomes less water-wet, residual saturation decreases and the capillary number increases [47]. The desaturation capillary curve for the oil-water system is strongly associated with wettability, as shown in Figure 17. The critical capillary or bond number for less water-wet rock is higher by at least one order of magnitude.

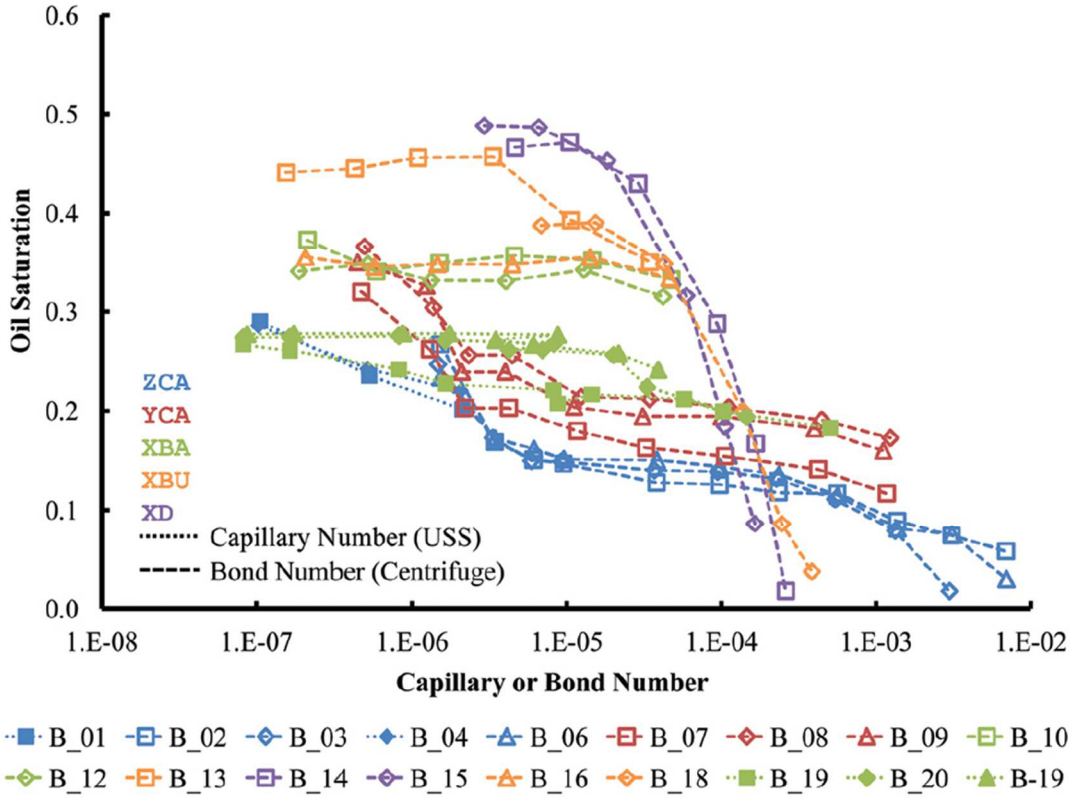

Figure 17 - Desaturation curve as a function of capillary or bond number in the oil-water system, for samples with different wettability [47].

The saline aquifer systems unaltered by hydrocarbons are considered water-wet with respect to CO_2-brine systems in typical reservoir conditions [48], [49].

The study of Baban 2023 [50] concludes that residual CO_2 trapping is substantially lower in oil-wet rocks than in analogous water-wet rocks.

3. METHODOLOGY

In this study, the goal is to evaluate the Capillary Desaturation Curve to understand the behaviour of the CO_2 trapping mechanism. Critical Capillary number is measured to know the minimum flow rate at which water displaces CO_2. Measurement of residual CO_2 saturation in a horizontal coreflood experiment is required. A relative permeability system is used to measure this parameter monitoring flow, pressure and temperature. CDC can be plotted as residual CO_2 saturation as a function of the Capillary/Bond/Trapping number.

3.1. LABORATORY EQUIPMENT

The tests are performed with the Relative Permeameter System RPS-700 designed by VINCI Technologies. The principal functions of this machine are the determination of effective permeability and residual saturations after flooding of core plugs using different fluids. All the parts in contact with the phases are made of Hastelloy to mitigate the risk of corrosion.

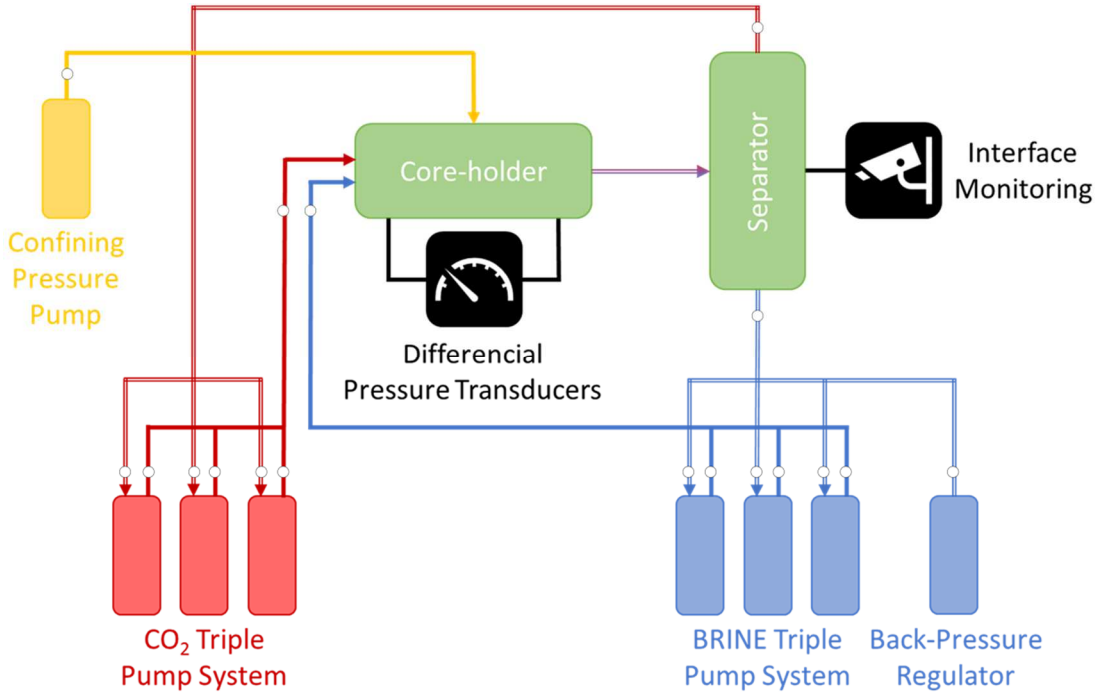

Figure 18 – Simplified machine scheme.

The main components are the following, as shown the Figure 20 [51].

- Injection Triple pump systems: two three-piston syringe pumps capable of continuous flow operation over a wide pressure range at reservoir temperature. Fluid delivery is possible at a constant rate or constant pressure. The three-piston configuration is required to guarantee a constant and continuous rate in a way to always have a piston pumping the fluid into the sample and one receiving it back from the downstream. However, an automatic system changes the pressure of the injecting piston according to the delta pressure on the core sample. When the permeability is low and, consequently, the delta pressure on the core is high, the pressure of the injecting piston must increase. When the pump needs to change the injecting piston, the pressure must be increased also for the new one, in order to maintain a continuous flow with a constant rate. The effects of this pressure adjustment are discussed in the section dedicated to the interpretation of the results.
- Hydrostatic core holder: core sample is held within a sleeve made of AFLAS by confining pressure (radial/axial stress), this simulates reservoir overburden pressure. Inlet and outlet end plugs allow fluids to be flooded through the core sample.
- Confining pressure pump: an automatic system to maintain a constant confining pressure.
- Fluid separator: it consists of a separator bore used to collect and separate produced immiscible fluids using gravity segregation and a measurement bore used to visualise the interface (through-window cell to allow the visibility of the fluids interface). The interface is measured continuously thanks to a video tracker system, it is able to monitor the interface position of the two fluids produced. If the interface inside the separator rises the volume of water increases and the value measured by the tracker system is positive. If the interface falls the volume of CO_2 increases and the measurement is negative.
- Back-pressure regulator: automatic pump filled with the same fluid used for the experiment (brine) that allows the pore pressure control.
- Heating system: two ovens (air baths) are used to heat the core holder and associated parts, using a forced air fan and heater, to perform the tests at a representative reservoir temperature. Temperature is controlled using a J-type thermocouple and digital controller.
- Pressure transducers: gauge-pressure transducers with digital displays. In a standard configuration, one monitors the confining pressure and two monitor the inlet and outlet pore pressure of the core.
- Differential pressure transducers: to monitor the difference between the inlet and the outlet pore pressure of the core sample. The first one measures 0.5 bar

at maximum with a sensitivity of 0.002 bar; on the other hand, the second one can measure up to 35 bar with a sensitivity of 0.01 bar.

- Software: all the equipment is controlled through a specific software installed on a computer, to allow automatic data acquisition.

All the components are joined by several tubings. To assess the correct volumes displaced from the core, the evaluation of the dead volume of the equipment is done. In this way, the fraction of water/CO_2 inside the separator due to the phase present inside the tubing is eliminated, summarized in Table 1.

Table 1: Dead volume measurements.

DEAD VOLUMES		
From	**To**	**Volume [cc]**
Core-holder inlet	Plug inlet	0.3
CO_2 triple pump system	Core-holder inlet	1.1
Water triple pump system	Core-holder inlet	1.0
Plug outlet	Core-holder outlet	2.1
Core-holder outlet	Separator inlet	3.3

3.2. SAMPLES AND FLUIDS

For the purposes of the study, two different core samples are used. The dry cores petrophysical properties are initially measured, and then, they are fully saturated with water, summarized in Table 2 [52].

- CORE A is a Medium-to-Fine Sandstone.

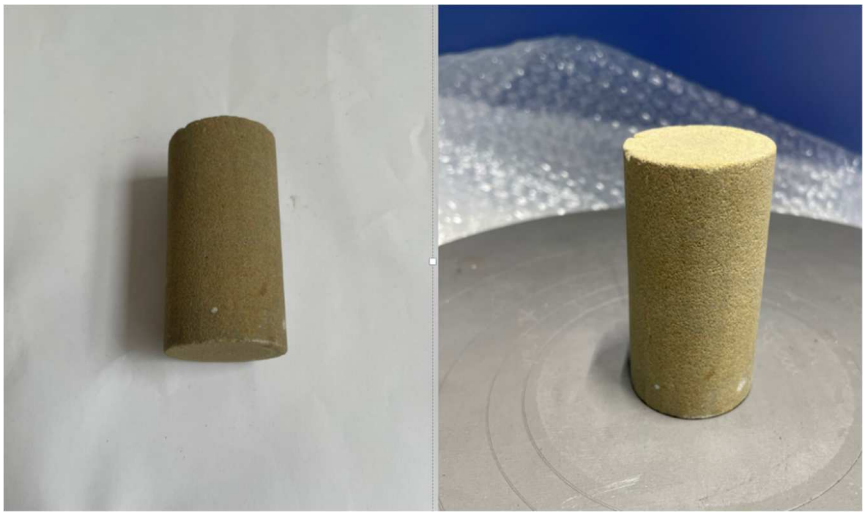

Figure 19 - Pictures of CORE A.

- CORE B is a Carbonate.

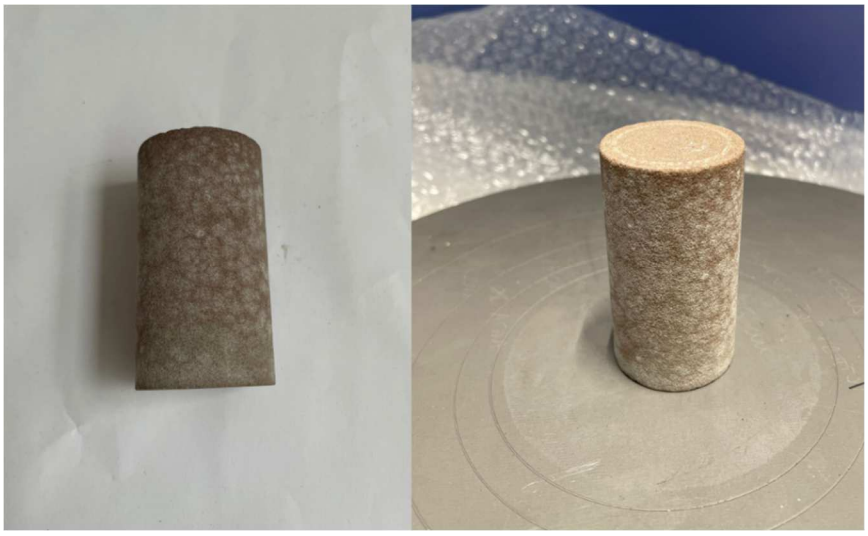

Figure 20 - Pictures of CORE B.

Table 2: Samples data [52].

PROPERTIES	CORE A	CORE B
Rock type	Medium-to-fine sandstone	Carbonate
Diameter [mm]	38	37.9
Length [mm]	73.9	69.3
Permeability [mD]	8.34	30.33
Porosity [%]	18.71	20.33
Bulk volume [cc]	83.81	78.18
Pore volume [cc]	15.681	15.894
Cross section [cm^2]	11.34	11.28
Irreducible water saturation [-]	0.61	0.38

The used fluids are CO_2 and water. The two phases are previously equilibrated to prevent mass transfer.

The pressure set in the separator is 105 bar for CORE A and 103.5 bar for CORE B.

The heating system maintains a temperature of 50 °C for both the tests.

All the properties of the fluids are calculated on the NIST portal [53] at these thermodynamic conditions, all the data are reported in Table 3.

The interfacial tension is taken from the literature [54]–[56], and is equal to 38 mN/m.

Table 3: Fluids properties.

PROPERTIES	CORE A	CORE B
Pressure [bar]	105	103.5
Temperature [°C]	50	50
Water density [kg/m^3]	992.52	992.46
Water viscosity [Pa*s]	0.00054864	0.00054861
CO_2 density [kg/m^3]	455.55	427.07
CO_2 viscosity [Pa*s]	0.000031726	0.000030466

3.3. EXPERIMENTAL PROCEDURE

The procedure of the test is the same for both the core samples, but different flow rate steps are used. The procedure is a discontinuous mode with step rates, as stated in Chapter 2.4.

1. The core is fully saturated by water and installed in the core folder.

2. CO_2 is injected for several hours to have a phase equilibration to evaluate the residual water saturation for setting the initial condition for water imbibition.

3. Water injection is done at increasing rates. During this stage, water enters the core plug and displaces the mobile CO_2 in the pores. The flow rate of water remains constant until a quasi-steady state is reached. The pressures, the interfacial level in the separator, and the volumes of water and CO2 present inside every piston of the pumps are continuously monitored and recorded every 10 seconds to have a complete view of the condition of the tested core sample.

In Table 4, the series of flow rate steps for each core is shown.

Table 4: Flow rate steps for each core.

CORE A	**CORE B**
Flow rate [cc/min]	
0.2	0.1
0.4	0.2
0.6	0.3
0.8	0.5
1	0.7
1.2	1
1.4	2
1.6	5
1.8	10
2	
2.2	
2.5	
3	
5	
7.5	
10	

4. RESULTS AND DISCUSSION

Firstly, the results of drainage are plotted to evaluate the initial saturations (residual water saturation and max CO_2 saturation). Then, water is injected at increasing rates until a quasi-steady state is reached to evaluate CO_2 residual saturation for each rate.

Fluid fractions present in the pore volume can be continuously monitored, thanks to the separator which measures the fluids exiting the sample, and, therefore, an easy evaluation of the saturation is possible. On the vertical axis the variation of volume inside the separator is plotted. If the height inside the separator rises the volume of water increases and the value measured by the tracker system is positive (during drainage test when CO_2 is injected). If the height falls the volume of CO_2 increases and the measurement is negative (during imbibition when water is injected).

A comparison between two different definitions of the Capillary number is done to evaluate the impact of the viscosity ratio. Bond and Trapping number is calculated for both Capillary number definitions. At the end, CDCs are plotted.

4.1. CORE A

In Figure 21 the results of the drainage test on the CORE A are plotted. A CO_2 injection with an increasing flow rate is done to evaluate the residual water saturation of the core. Initial fluid displaced is the dead volume of the equipment, for this reason, a volume of 5.7 cc is subtracted from the volume measured in the separator. All the negative values are removed and a filter with a tolerance of 0.2 cc is applied. The stabilization of the curve is 6 cc (pore volume = 15.68 cc)., the CO_2 saturation is 38.3% and the residual water saturation is 61.7%. The final condition of the drainage test represents the initial one of the imbibition test, the volumes inside the pores and fluid saturations after the drainage test are summarized in Table 5.

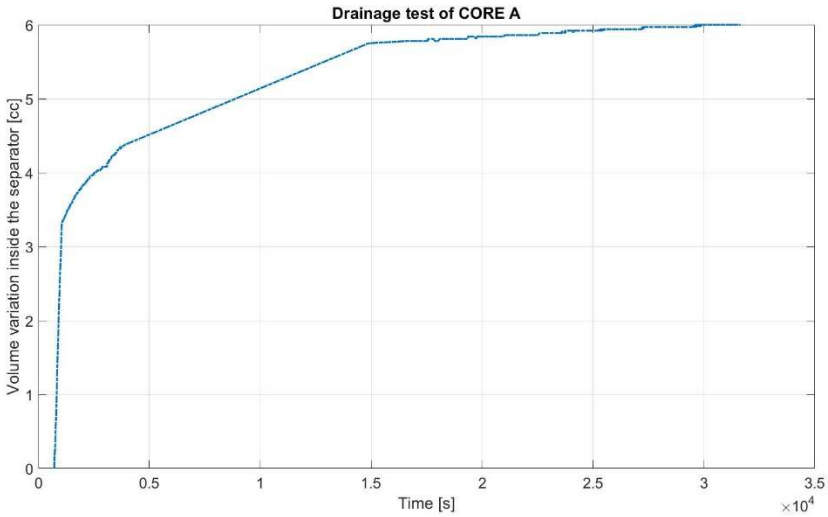

Figure 21 - Drainage test plot of CORE A.

Table 5: Results of drainage test for CORE A.

Irreducible water saturation [-]	0.61
Maximum CO_2 saturation [-]	0.39
Initial volume of water [cc]	9.57
Initial volume of CO2 [cc]	6.12

In Figure 22, the results of the tests on the CORE A are plotted. Each colour corresponds to a specific constant flow rate of the test.

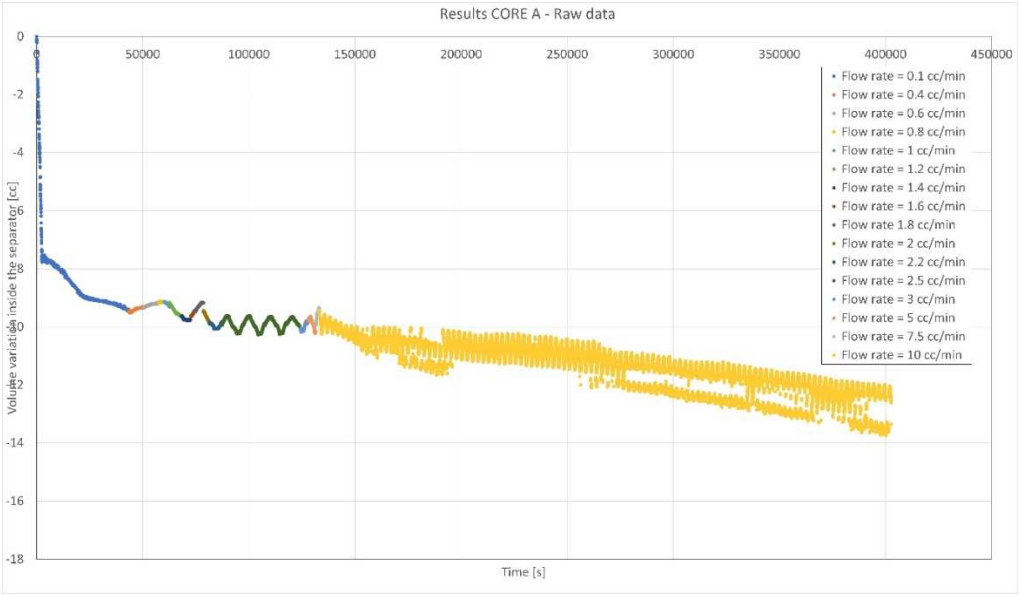

Figure 22 - Plot of the continuous variation of the volume inside the separator in time, raw results for CORE A.

The relative permeability system maintains a constant flow rate by automatically adjusting the pressure of the system. When the water pump changes the piston, the new pumping piston is pressurized at the injection pressure of the previous one. The equilibration of the system changes the height of the phases interface inside the separator and measures the wrong amount of water present inside the core. The oscillation of the data is due to the pressure adjustment when the injecting water pump is shifted. This effect is higher in the core with low permeability, as it will be presented in Chapter 4.2 involving a more permeable sample, where this effect is less significant. It is possible to eliminate the effect of this phenomenon by calculating the initial volume of water in the three water pumps and un the BPR pump and subtracting this value for the current volume of water in these four pumps, using Eq. 10 - 11. This variation can be added to the estimation of the separator and the correct amount of water and CO_2 inside the core is measured. The initial volume is calculated every time that the interface of the separator is put to zero, for the CORE A every time that the flow rate is changed. Initial volume changes for each flow rate step. In the interpretation section also, this effect is adjusted to have a realistic result before the evaluation of the Capillary Desaturation Curve.

$$V_{initial} = V_{P1\,water} + V_{P2\,water} + V_{P3\,water} + V_{BPR} \qquad \text{Eq. 10}$$

$$\Delta V_{separator}^{corrected} = \Delta V_{separator}^{measured} + V_{initial} \qquad \text{Eq. 11}$$

The first step of the interpretation is the reduction of the data scattering due to the uncertainty of tracker measurement of the interface inside the separator. The smoother curve, plotted in Figure 23, is calculated using an arithmetic average of the 5000 points before and after for each point. In the first one, the average is calculated only for the 5000 points after, instead, for the following points gradually of the points before and the 5000 points after, until the complete average algorithm becomes suitable. The same principle is applied to the last points.

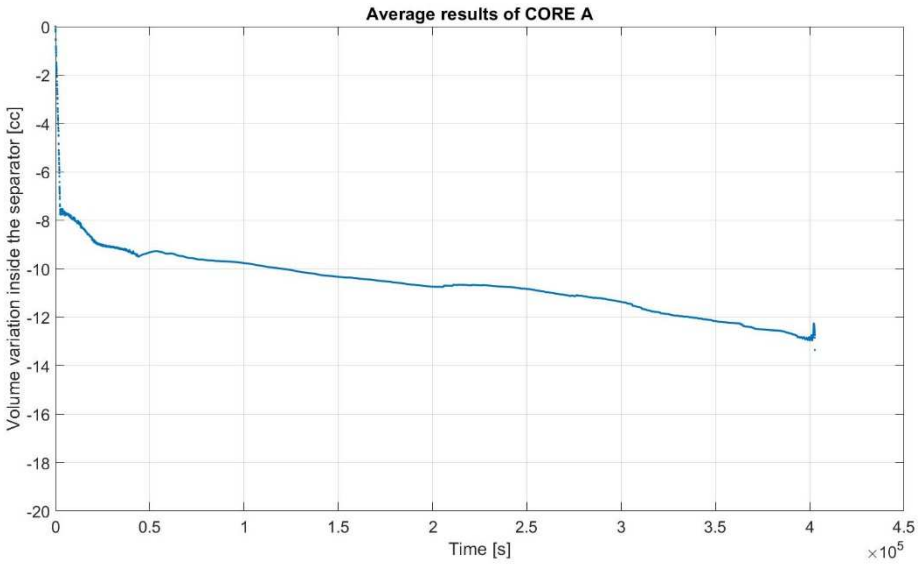

Figure 23 - Average results of CORE A.

The following step is transforming the curve into a monotonically decreasing one. The effect of the uncertainty of the tracker measurement is not totally eliminated. To enhance the estimation of the CO_2 and water volumes inside the separator the data are thinned out. A point every 50 points is recorded in the thinned curve.

Then Eq. 12 is used to transform the curve into a monotonic decreasing one. In which i is a generic point of the curve, A is the initial thinned data and B is the final thinned data monotonic decreasing, plotted in Figure 24.

$$\begin{cases} B_i = B_{i-1} & if\ A_i \geq A_{i-1} \\ B_i = B_{i-1} + (A_i - A_{i-1}) & if\ A_i < A_{i-1} \end{cases} \qquad \text{Eq. 12}$$

If the data is higher than the previous one, it is replaced with the previous one. If the data is lower, it is replaced with the previous one summed with the negative variation, to add every contribution of the volume displaced.

The last long part of the test with a flow rate of 10 cc/min is truncated because of the fluctuation of the data due to the pump adjustment being too strong.

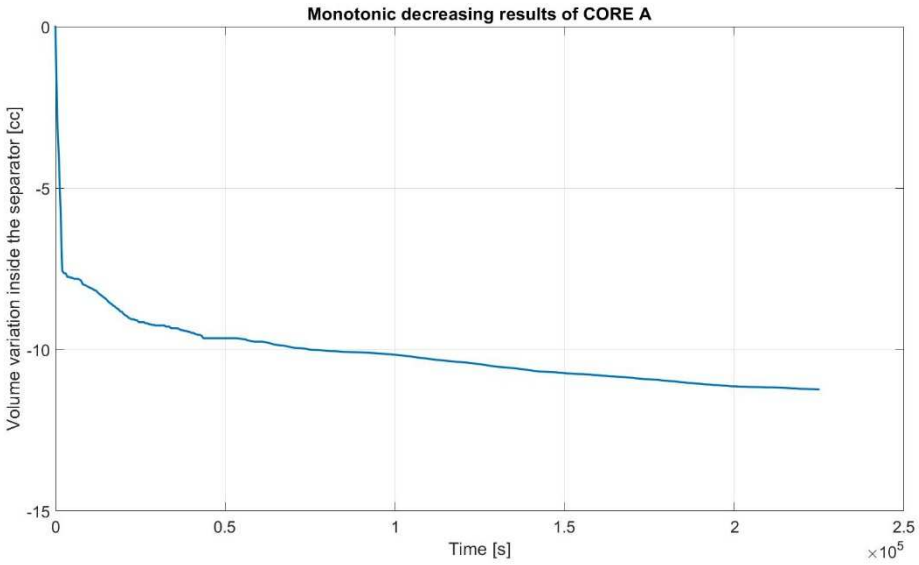

Figure 24 - Monotonic increasing results of CORE A.

The final data (red point in Figure 25) for each flow rate step is acquired and used to calculate the volume of CO_2 displaced during the test.

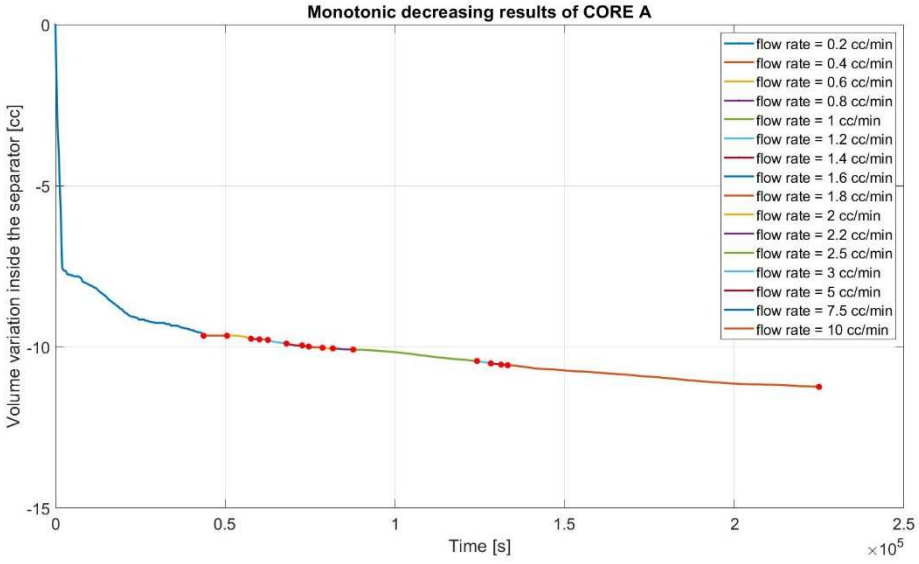

Figure 25 - Monotonic decreasing results of CORE A, with the recorded points (redpoint) for each flow rate.

The results of each test and the corresponding residual CO_2 saturation calculated are summarized in Table 6.

Table 6: Results of imbibition tests for CORE A..

RATE [cc/min]	Volume variation inside the separator (red point in Figure 26) [cc]	Corrected by Dead volume	CO2 in CORE A [cc]	Water in CORE A [cc]	Residual CO2 saturation [-]
0.2	-9.6496	-4.2496	1.866	13.815	0.119
0.4	-9.6494	-4.2494	1.866	13.815	0.119
0.6	-9.7425	-4.3425	1.773	13.908	0.113
0.8	-9.759	-4.359	1.757	13.924	0.112
1	-9.7908	-4.3908	1.725	13.956	0.110
1.2	-9.8993	-4.4993	1.616	14.065	0.103
1.4	-9.9621	-4.5621	1.553	14.127	0.099
1.6	-9.9983	-4.5983	1.517	14.164	0.097
1.8	-10.026	-4.626	1.490	14.191	0.095
2	-10.0514	-4.6514	1.464	14.217	0.093
2.2	-10.0825	-4.6825	1.433	14.248	0.091
2.5	-10.4462	-5.0462	1.069	14.612	0.068
3	-10.5066	-5.1066	1.009	14.672	0.064
5	-10.5414	-5.1414	0.974	14.707	0.062
7.5	-10.5615	-5.1615	0.954	14.727	0.061
10	-11.2404	-5.8404	0.275	15.406	0.018

Residual CO_2 saturation is calculated starting from the initial volume of CO_2 and water present in the core. The volume variation inside the separator corresponds to the volume of water or CO_2 displaced in the core. The variation in the separator is negative, the interphase goes down the CO_2 inside the separator increases, and the CO_2 inside the core decreases. Before the calculation, the dead volume of 5.4 cc is subtracted.

The capillary number is calculated with Eq. 2 (v: velocity, μ: viscosity, σ: interfacial tension) and Eq. 4 (v: velocity, μ_{water}: water viscosity, μ_{oil}: oil viscosity σ: interfacial tension). The first one is the classical simplest definition, the second one includes the viscosity ratio. These two definitions are used to assess the impact of viscosity ratio on Capillary number.

$$N_{cap} = \frac{v\,\mu_{water}}{\sigma} \qquad \text{Eq. 2}$$

$$N_{cap} = \frac{v\,\mu_{water}}{\sigma}\left(\frac{\mu_{water}}{\mu_{oil}}\right)^{0.4} \qquad \text{Eq. 4}$$

Bond number is calculated with the analytical definition Eq. 7 (K: absolute permability, Δρ: density difference between displacing and displaced phases, g: gravity acceleration). The contact angle is 85° [54].

$$N_{bond} = \frac{\mathrm{K}\,\Delta\rho\,g}{\phi\,\sigma\cos(\theta)} \qquad \text{Eq. 7}$$

The trapping number is calculated with Eq. 8 (θ is the angle from the horizontal level). In the equipment the core is horizontal ($\theta = 0$).

$$N_{trap} = \sqrt{N_{cap}^2 + 2\,N_{cap}N_{bond}\sin(\theta) + N_{bond}^2} \qquad \text{Eq. 8}$$

In Figure 26 the residual CO_2 saturation for CORE A is plotted as a function of the classical definition of the Capillary number (Eq. 3) and the Abrams definition including viscosity ratio (Eq. 8).

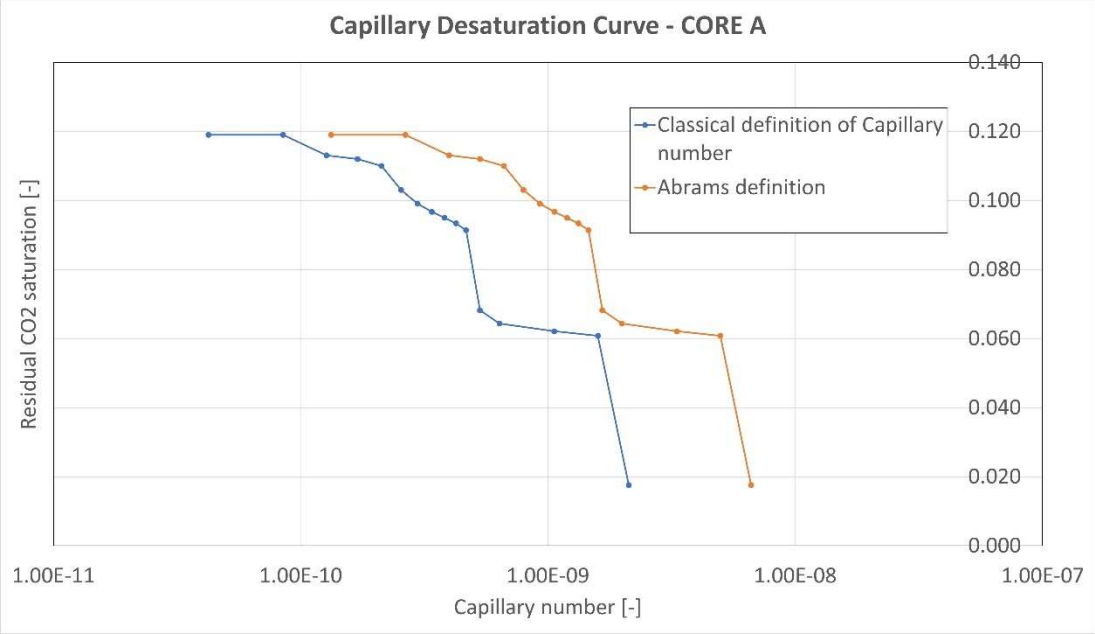

Figure 26 - Capillary desaturation curve for CORE A using Capillary number.

The critical Capillary number for CORE A is about 2E-10.

The Bond Number (Eq. 7) is 6.99E-11.

In Figure 27 the residual CO_2 saturation for CORE A is plotted as a function of the Trapping number calculated using both the classical definition of Capillary number and the Abrams definition.

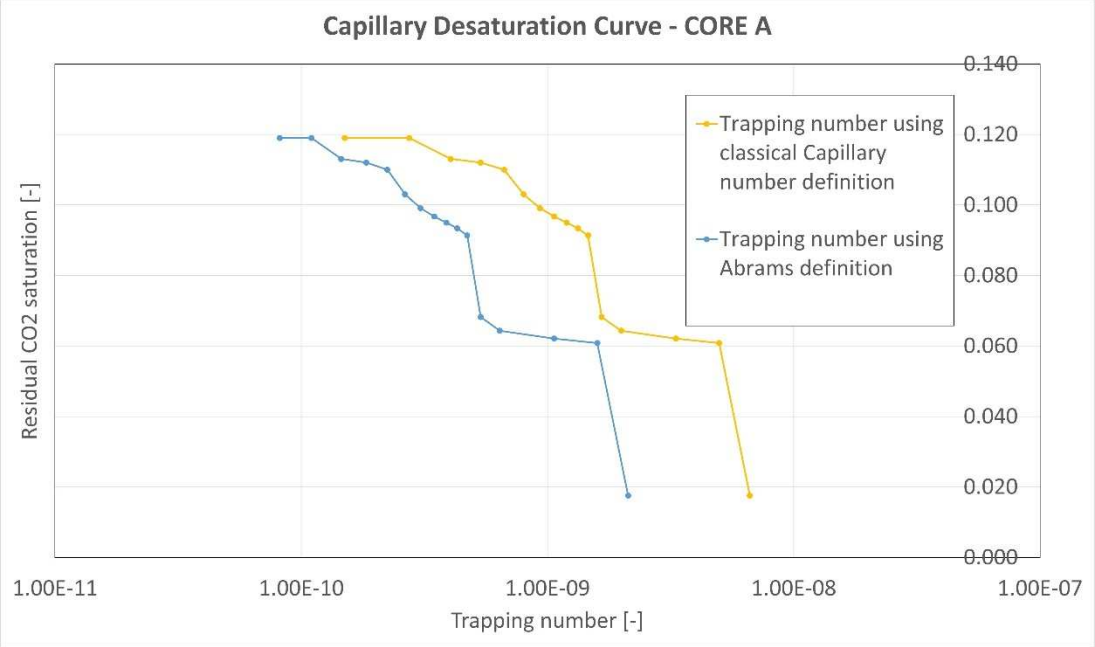

Figure 27 - Capillary desaturation curve for CORE A using Trapping number.

The difference between the CDC plotted with Capillary and Trapping number is almost negligible due to the relatively high flow rate used that dominates the gravitational effects.

4.2. CORE B

In Figure 28 the results of the drainage test on the CORE B are plotted. CO_2 is injected as for CORE A, to evaluate the residual water saturation. The stabilization of the curve is 9.6 cc (pore volume = 15.89 cc)., the CO_2 saturation is 60.4% and the residual water saturation is 39.6%. The final condition of the drainage test represents the initial one of the imbibition test, the volumes inside the pores and fluid saturations after the drainage test are summarized in Table 7.

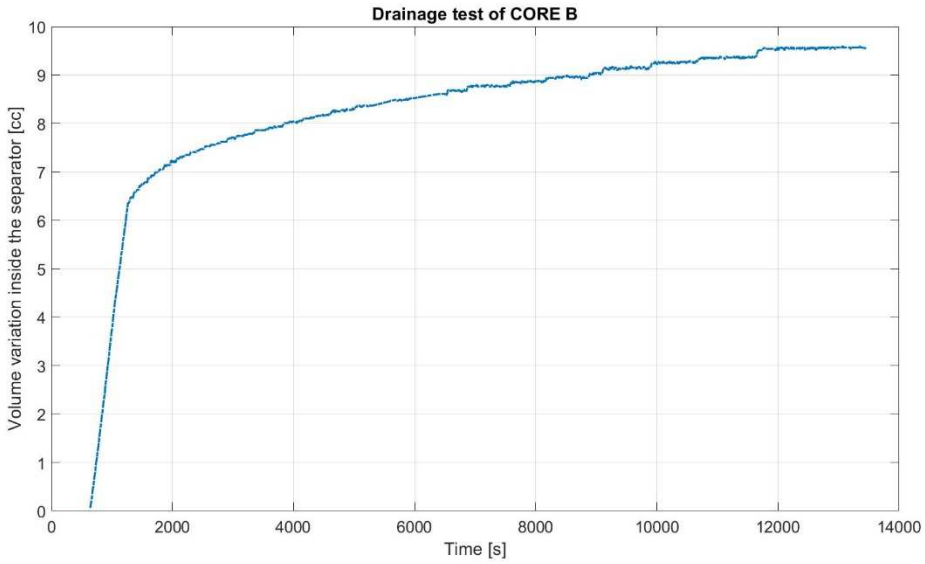

Figure 28 - Plot of the volume variation inside the separator in time during the drainage test for CORE B.

Table 7: Results of drainage test for CORE B.

Irreducible water saturation [-]	0.38
Maximum CO_2 saturation	0.62
Initial volume of water [cc]	6.04
Initial volume of CO2 [cc]	9.85

In Figure 29, the results of the tests on the CORE B are plotted. For CORE B, the volume inside the separator is put to zero only before the start. Each colour corresponds to a specific constant flow rate of the test, as reported in Table 4. The scattered data for the third part of the test of 0.3 cc/min are due to the pump adjustment as explained for CORE A. It is possible to see the same effect during the last parts of the test. CORE B has a higher permeability than CORE A, this is shown in the lower scattering of the data due to the changing pressure of the system. In the interpretation

section the test at 0.3 cc/min is interpolated with a smoothed function and the effect of pump adjustment is corrected using Eq. 10 – 11. The initial volume is calculated every time that the interface of the separator is put to zero, for the CORE B only before the starting point of the test. The initial volume is the same for all the flow rate steps.

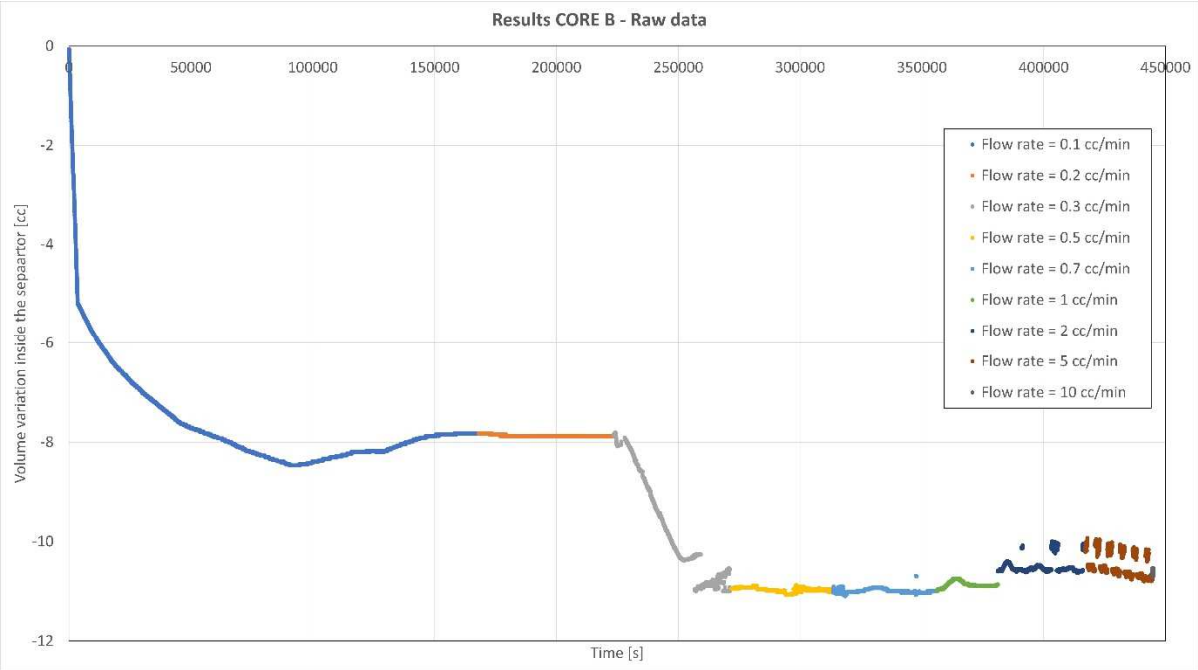

Figure 29 - Plot of the continuous variation of the volume inside the separator in time, raw results for CORE B.

The same interpretation procedure used for CORE A is applied for CORE B.

The discontinuity of the test at 0.3 cc/min is plotted as a polynomial function of 3° grade that interpolates a suitable interval of points before and after the discontinuity as shown in Figure 30.

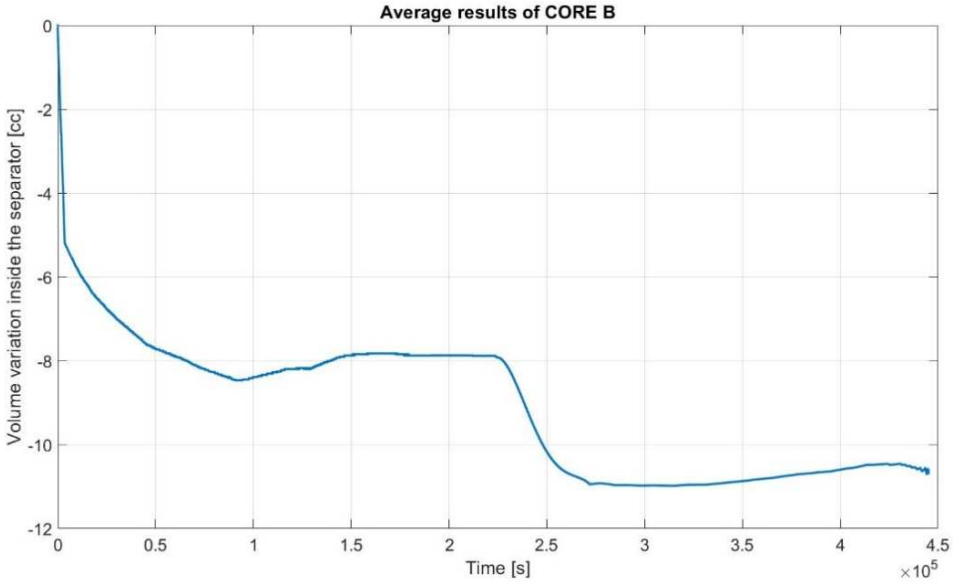

Figure 30 - Average results of CORE B.

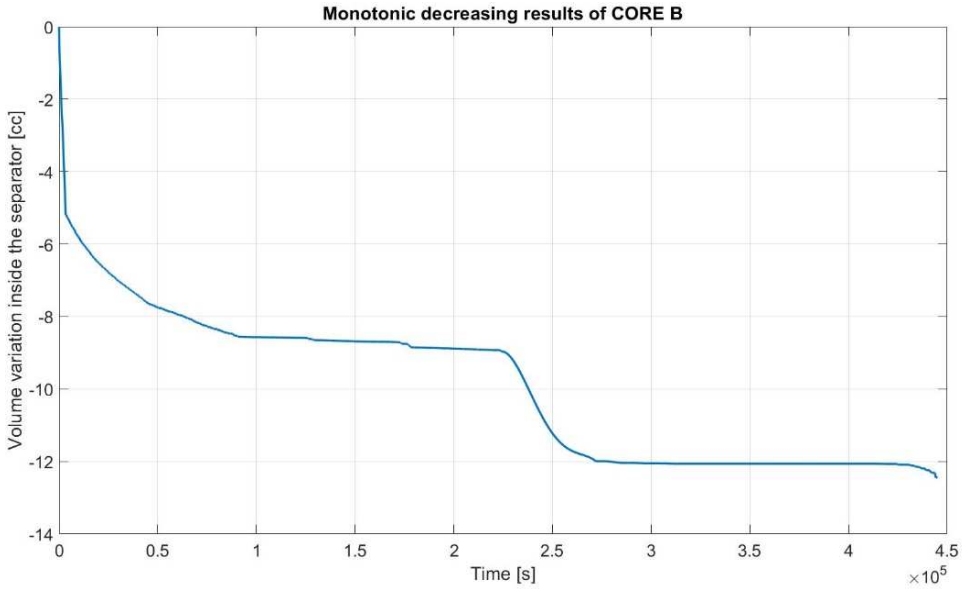

Figure 31 - Monotonic decreasing results of CORE B.

In Figure 31, the data are thinned, and Eq. 12 is applied to have a monotonic decreasing curve. The last two tests are deleted because of the effect of the pump adjustment.

The final data (red point in Figure 32) for each flow rate step is acquired and used to calculate the volume of CO_2 displaced during the test.

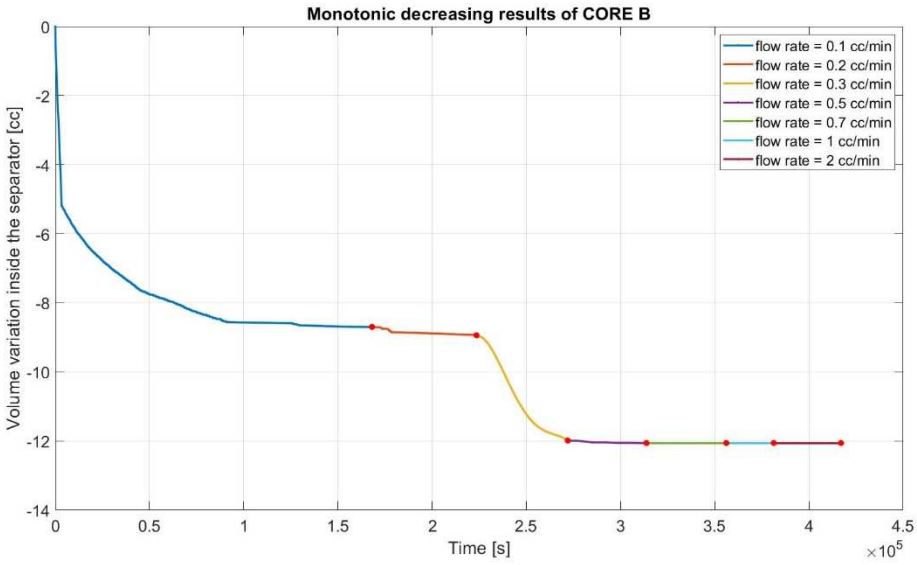

Figure 32 - Monotonic decreasing results of CORE B, with the recorded points (redpoint) for each flow rate.

The results of each test and the corresponding residual CO_2 saturation calculated are summarized in Table 8.

Table 8: Results of imbibition tests for CORE B.

RATE [cc/min]	Volume variation inside the separator (red point in Figure 30) [cc]	Corrected by Dead Volume [cc]	CO2 in CORE B [cc]	Water in CORE B [cc]	Residual CO2 saturation [-]
0.1	-8.704	-3.304	6.550	9.344	0.412
0.2	-8.935	-3.535	6.319	9.575	0.398
0.3	-11.9954	-6.5954	3.259	12.635	0.205
0.5	-12.0646	-6.6646	3.190	12.704	0.201
0.7	-12.0647	-6.6647	3.190	12.704	0.201
1	-12.0647	-6.6647	3.190	12.704	0.201
2	-12.0669	-6.6669	3.187	12.707	0.201

The residual CO_2 saturation is calculated starting from the initial volume of CO_2 and water present in the core. The volume variation inside the separator corresponds to the volume of water or CO_2 displaced in the core. The variation in the separator is negative, the interphase goes down the CO_2 inside the separator increases, and the CO_2 inside the core decreases. Before the calculation, the dead volume correction is applied.

Capillary/Bond/Trapping numbers are calculated using the same definition applied for CORE A, reported in Chapter 4.1.

In Figure 33 the residual CO_2 saturation for CORE B is plotted as a function of the classical definition of the Capillary number (Eq. 3) and the Abrams definition including viscosity ratio (Eq. 8).

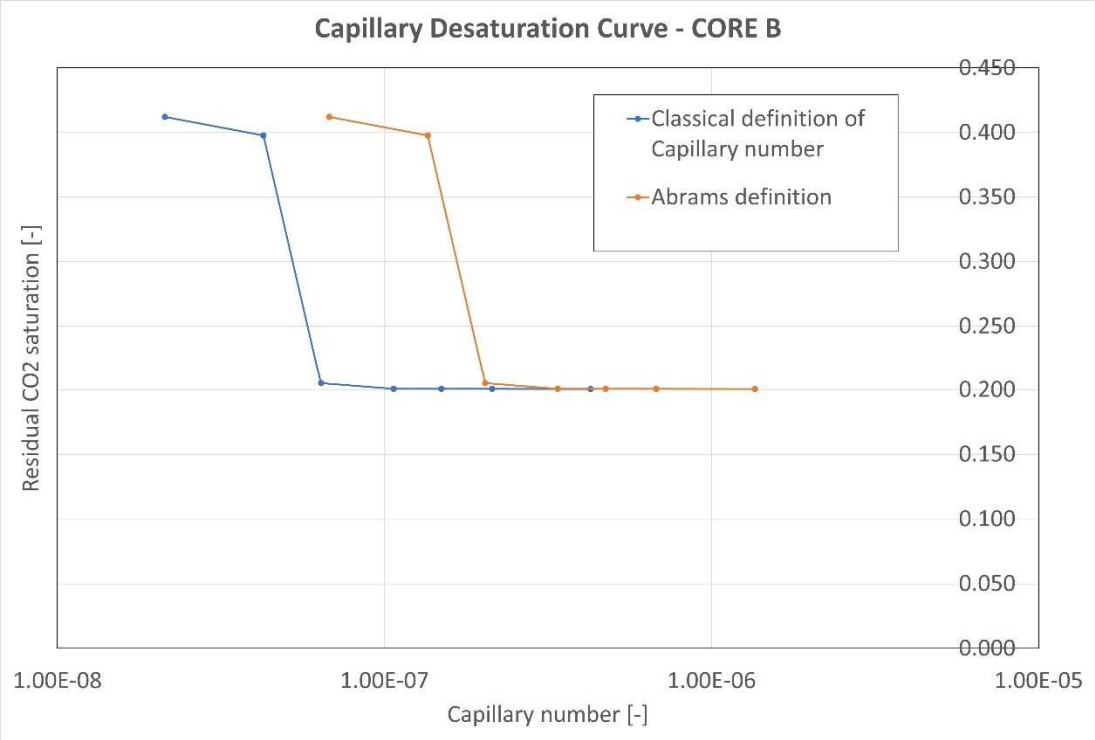

Figure 33 - Capillary desaturation curve for CORE B using Capillary number.

The critical Capillary number for CORE B is about 4 E-8.

The Bond number is 2.46E-10.

In Figure 34 the residual CO_2 saturation for CORE B is plotted as a function

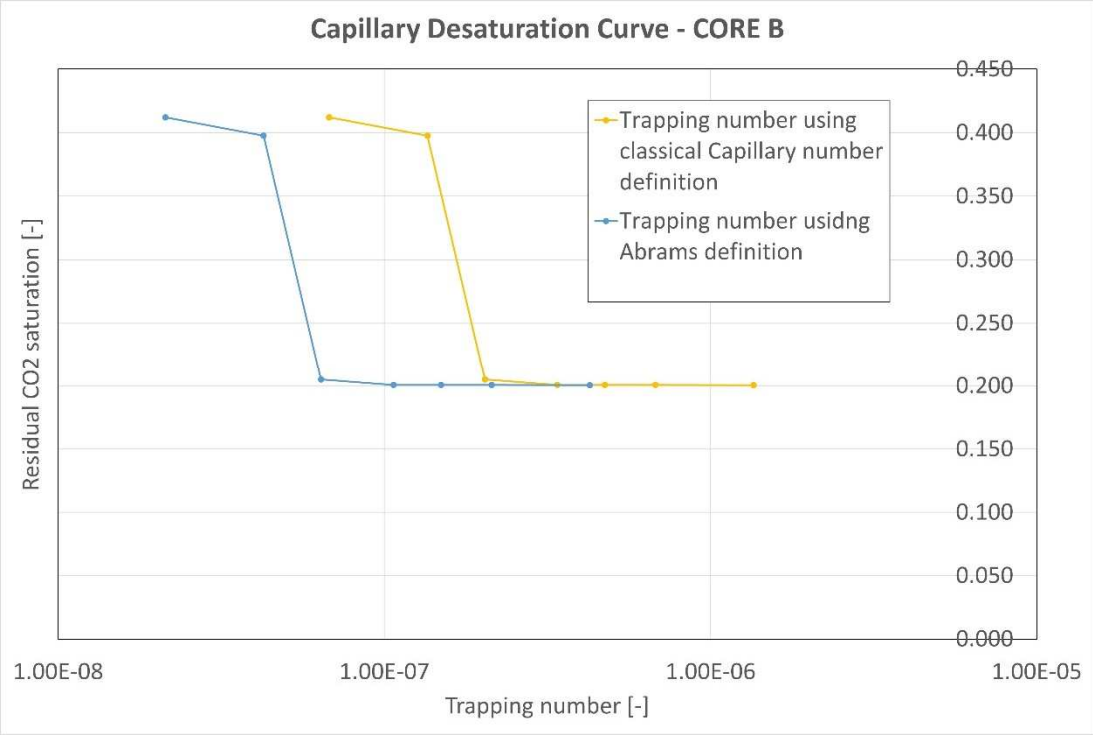

Figure 34 - Capillary desaturation curve for CORE B using Trapping number.

Also in this case, the difference between the CDC plotted with Capillary and Trapping number is almost negligible due to the relatively high flow rate used that dominates the gravitational effects.

5. CONCLUSIONS

This thesis presents the results of core flooding experiments of a CO_2-water system for two rock samples, a sandstone and a carbonate. The scope of this study is to better characterize the capillary trapping mechanism during carbon dioxide injection in a deep saline aquifer.

Residual CO_2 saturation is calculated from the results of the imbibition tests and Capillary Desaturation Curves are plotted for each core as a function of Capillary and Trapping number.

The trend of the CDCs is consistent with what is expected, and coherent with what is presented in literature in other studies. CDCs of this work represent a classical Capillary Desaturation Curve for a CO_2-water system.

During CO_2 injection, the goal is to maximise the trapped carbon dioxide. According to the Capillary Desaturation Curve, one possible strategy can be an additional water injection at a low rate to push slowly the CO_2 plume and enhance the imbibition process that increases the fraction of trapped carbon dioxide.

Capillary number choice has a huge impact on the Capillary Desaturation Curve. Two definitions of Capillary number are used, to assess the impact of viscosity ratio. Results show a non-negligible variation, due to the different viscosity of the fluids.

Comparing the results between sandstone and carbonate, it can be deduced that the carbonate CDCs is steeper than the sandstone one, as it is expected.

The values of the Critical Capillary number were not coherent with what was expected. The critical Capillary number should decrease if the permeability increases. Instead, the more permeable core presents a higher critical capillary number probably due to the different rock types.

As expected, when the injection rates are high, gravitational effects become negligible. Trapping and Capillary numbers have the same order of magnitude.

The effects of solubility, salinity and contact angle were not assessed in this work because the experiments are extremely long (in the order of weeks), so further investigations would be needed to assess the impact of these parameters on the Critical Capillary number.

REFERENCES

[1] C. Benetatos, E. S. Borello, C. Peter, V. Rocca, and R. Romagnoli, 'Considerations on energy transition', 2019, doi: https://hdl.handle.net/11583/2812471.

[2] Wikipedia, 'United Nations Framework Convention on Climate Change'. [Online]. Available: https://en.wikipedia.org/wiki/United_Nations_Framework_Convention_on_Climate_Change

[3] Wikipedia, 'United Nations Climate Change conference'. [Online]. Available: https://en.wikipedia.org/wiki/United_Nations_Climate_Change_conference

[4] M. Zupi, 'Aggiornamento sulle sfide climatiche a seguito della COP27', Feb. 2023.

[5] 'The European Green Deal - COMMUNICATION FROM THE COMMISSION TO THE EUROPEAN PARLIAMENT, THE EUROPEAN COUNCIL, THE COUNCIL, THE EUROPEAN ECONOMIC AND SOCIAL COMMITTEE AND THE COMMITTEE OF THE REGIONS', European Commission, Brussels, Dec. 2019.

[6] European Commission, 'Delivering the European Green Deal'. Oct. 20, 2023. [Online]. Available: https://commission.europa.eu/strategy-and-policy/priorities-2019-2024/european-green-deal/delivering-european-green-deal_en

[7] European commission, 'SETIS - SET Plan information system'. Oct. 2023. [Online]. Available: https://setis.ec.europa.eu/implementing-actions/ccs-ccu_en

[8] 'Carbon Capture, Utilisation and Storage', International Energy Agency, Jul. 2023. [Online]. Available: https://www.iea.org/energy-system/carbon-capture-utilisation-and-storage

[9] Carbon Capture & Storage Association, 'CCUS Roadmap to 2023 - CCUS SET-PLAN', European Commission, Oct. 2021.

[10] United Nations Department of Economic and Social Affairs, *The Sustainable Development Goals Report 2023: Special Edition*. in The Sustainable Development Goals Report. United Nations, 2023. doi: 10.18356/9789210024914.

[11] 'CCUS - Net Zero Emissions Guide', International Energy Agency, Sep. 2023. [Online]. Available: https://www.iea.org/reports/ccus

[12] 'Global status of CCS 2022', Global CCS Institute, 2022.

[13] F. Verga, 'Storage capacity, working gas and cushion gas, deliverability', Jan. 2023.

[14] 'Carbon Dioxide Capture and Storage - IPCC 2005', Intergovernmental Panel on Climate Change, 2005.

[15] C. H. Pentland, R. El-Maghraby, A. Georgiadis, S. Iglauer, and M. J. Blunt, 'Immiscible Displacements and Capillary Trapping in CO2 Storage', *Energy Procedia*, vol. 4, pp. 4969–4976, 2011, doi: 10.1016/j.egypro.2011.02.467.

[16] R. Qi, T. Laforce, and M. Blunt, 'Design of carbon dioxide storage in aquifers', *International Journal of Greenhouse Gas Control*, vol. 3, no. 2, pp. 195–205, Mar. 2009, doi: 10.1016/j.ijggc.2008.08.004.

[17] M. A. Hesse, F. M. Orr Jr., and H. A. Tchelepi, 'Gravity currents with residual trapping', *Energy Procedia*, vol. 1, no. 1, pp. 3275–3281, Feb. 2009, doi: 10.1016/j.egypro.2009.02.113.
[18] R. Lenormand and C. Zacone, 'Physics of Blob Displacement in a Two-Dimensional Porous Medium', *SPE Formation Evaluation*, vol. 3, no. 01, pp. 271–275, Mar. 1988, doi: 10.2118/14882-PA.
[19] L. Yu (Y. Li) and N. C. Wardlaw, 'Mechanisms of nonwetting phase trapping during imbibition at slow rates', *Journal of Colloid and Interface Science*, vol. 109, no. 2, pp. 473–486, Feb. 1986, doi: 10.1016/0021-9797(86)90325-5.
[20] S. Krevor, C. Reynolds, A. Al-Menhali, and B. Niu, 'The Impact of Reservoir Conditions and Rock Heterogeneity on CO2-Brine Multiphase Flow In Permeable Sandstone', 2016.
[21] H. Guo, K. Song, and R. Hilfer, 'A Brief Review of Capillary Number and its Use in Capillary Desaturation Curves', *Transp Porous Med*, vol. 144, no. 1, pp. 3–31, Aug. 2022, doi: 10.1007/s11242-021-01743-7.
[22] P. G. Saffman and G. I. Taylor, 'The penetration of a fluid into a porous medium or Hele-Shaw cell containing a more viscous liquid', 1958, doi: https://doi.org/10.1098/rspa.1958.0085.
[23] T. W. Teklu, J. S. Brown, H. Kazemi, R. M. Graves, and A. M. AlSumaiti, 'Residual Oil Saturation Determination – Case Studies in Sandstone and Carbonate Reservoirs', presented at the EAGE Annual Conference & Exhibition incorporating SPE Europec, Jun. 2013, p. SPE-164825-MS. doi: 10.2118/164825-MS.
[24] H. Guo *et al.*, 'Review of Capillary Number in Chemical Enhanced Oil Recovery', presented at the SPE Kuwait Oil and Gas Show and Conference, Oct. 2015, p. SPE-175172-MS. doi: 10.2118/175172-MS.
[25] H. Guo, K. Song, and R. Hilfer, 'A Critical Review of Capillary Number and its Application in Enhanced Oil Recovery', presented at the SPE Improved Oil Recovery Conference, Aug. 2020, p. D031S046R001. doi: 10.2118/200419-MS.
[26] S. K. Masalmeh, 'Determination of Waterflooding Residual Oil Saturation for Mixed to Oil-Wet Carbonate Reservoir and its Impact on EOR', presented at the SPE Reservoir Characterization and Simulation Conference and Exhibition, Sep. 2013, p. SPE-165981-MS. doi: 10.2118/165981-MS.
[27] L. Lake, R. T. Johns, W. R. Rossen, and G. A. Pope, *Fundamentals of Enhanced Oil Recovery*. Society of Petroleum Engineers. doi: 10.2118/9781613993286.
[28] T. F. Moore and R. L. Slobod, 'Displacement of Oil by Water-Effect of Wettability, Rate, and Viscosity on Recovery', presented at the Fall Meeting of the Petroleum Branch of AIME, Oct. 1955, p. SPE-502-G. doi: 10.2118/502-G.
[29] A. Abrams, 'The Influence of Fluid Viscosity, Interfacial Tension, and Flow Velocity on Residual Oil Saturation Left by Waterflood', *Society of Petroleum Engineers Journal*, vol. 15, no. 05, pp. 437–447, Oct. 1975, doi: 10.2118/5050-PA.
[30] S. Doorwar and K. K. Mohanty, 'Viscous-Fingering Function for Unstable Immiscible Flows', *SPE Journal*, vol. 22, no. 01, pp. 019–031, Feb. 2017, doi: 10.2118/173290-PA.
[31] S. R. McDougall and K. S. Sorbie, 'The Combined Effect of Capillary and Viscous Forces on Waterflood Displacement Efficiency in Finely Laminated

Porous Media', presented at the SPE Annual Technical Conference and Exhibition, Oct. 1993, p. SPE-26659-MS. doi: 10.2118/26659-MS.
[32] A. Georgiadis, S. Berg, A. Makurat, G. Maitland, and H. Ott, 'Pore-scale micro-computed-tomography imaging: Nonwetting-phase cluster-size distribution during drainage and imbibition', *Phys. Rev. E*, vol. 88, no. 3, p. 033002, Sep. 2013, doi: 10.1103/PhysRevE.88.033002.
[33] M. J. King, A. J. Falzone, W. R. Cook, J. W. Jennings Jr., and W. H. Mills, 'Simultaneous Determination of Residual Saturation and Capillary Pressure Curves Utilizing the Ultracentrifuge', presented at the SPE Annual Technical Conference and Exhibition, Oct. 1986, p. SPE-15595-MS. doi: 10.2118/15595-MS.
[34] M. Jin, 'A study of nonaqueous phase liquid characterization and surfactant remediation', The University of Texas at Austin, Texas, USA, 1995.
[35] C. Chang, T. J. Kneafsey, Q. Zhou, M. Oostrom, and Y. Ju, 'Scaling the impacts of pore-scale characteristics on unstable supercritical CO2-water drainage using a complete capillary number', *International Journal of Greenhouse Gas Control*, vol. 86, pp. 11–21, Jul. 2019, doi: 10.1016/j.ijggc.2019.04.010.
[36] A. Siyal, K. Rahimov, W. AlAmeri, and E. W. Al-Shalabi, 'Recent Advances in Capillary Desaturation Curves for Sandstone and Carbonate Reservoirs', in *Day 1 Mon, November 15, 2021*, Abu Dhabi, UAE: SPE, Dec. 2021, p. D012S141R001. doi: 10.2118/207595-MS.
[37] A. Siyal, K. Rahimov, W. AlAmeri, E. W. Al-Shalabi, and S. Ahmed, 'A Comprehensive Review on the Capillary Desaturation Curves for Sandstone and Carbonate Reservoirs', *SPE Reservoir Evaluation & Engineering*, vol. 26, no. 03, pp. 651–675, Aug. 2023, doi: 10.2118/207595-PA.
[38] J. M. Garnes, A. M. Mathisen, A. Scheie, and A. Skauge, 'Capillary Number Relations for Some North Sea Reservoir Sandstones', presented at the SPE/DOE Enhanced Oil Recovery Symposium, Apr. 1990, p. SPE-20264-MS. doi: 10.2118/20264-MS.
[39] J. S. Tang and B. Harker, 'Interwell Tracer Test To Determine Residual Oil Saturation In A Gas-Saturated Reservoir. Part I: Theory And Design', *Journal of Canadian Petroleum Technology*, vol. 30, no. 03, May 1991, doi: 10.2118/91-03-08.
[40] M. Ding and A. Kantzas, 'Capillary Number Correlations for Gas-Liquid Systems', 2004.
[41] I. Chatzis and N. R. Morrow, 'Correlation of Capillary Number Relationships for Sandstone', *Society of Petroleum Engineers Journal*, vol. 24, no. 05, pp. 555–562, Oct. 1984, doi: 10.2118/10114-PA.
[42] M. Ding and A. Kantzas, 'Investigation of Critical Capillary Number for Gas-Water System Through Experiment and Reservoir Simulation', 2005.
[43] Y. Wang *et al.*, 'Experimental Study of Crossover from Capillary to Viscous Fingering for Supercritical CO2–Water Displacement in a Homogeneous Pore Network', *Environ. Sci. Technol.*, vol. 47, no. 1, pp. 212–218, Jan. 2013, doi: 10.1021/es3014503.
[44] C. Zhang, M. Oostrom, T. W. Wietsma, J. W. Grate, and M. G. Warner, 'Influence of Viscous and Capillary Forces on Immiscible Fluid Displacement: Pore-Scale Experimental Study in a Water-Wet Micromodel Demonstrating

Viscous and Capillary Fingering', *Energy Fuels*, vol. 25, no. 8, pp. 3493–3505, Aug. 2011, doi: 10.1021/ef101732k.
[45] R. Hilfer, R. T. Armstrong, S. Berg, A. Georgiadis, and H. Ott, 'Capillary saturation and desaturation', *Phys. Rev. E*, vol. 92, no. 6, p. 063023, Dec. 2015, doi: 10.1103/PhysRevE.92.063023.
[46] L. Anton and R. Hilfer, 'Trapping and mobilization of residual fluid during capillary desaturation in porous media', *Phys. Rev. E*, vol. 59, no. 6, pp. 6819–6823, Jun. 1999, doi: 10.1103/PhysRevE.59.6819.
[47] K. J. Humphry, 'Impact of Wettability on Residual Oil Saturation and Capillary Desaturation Curves', 2014.
[48] A. Al-Menhali, S. Krevor, and Q. Carbonates, 'Remaining Saturations of Supercritical CO2 in Mixed-wet Carbonates for Carbon Utilization in Oil Fields: Core to Pore Scales Observations and Field Scale Implications', in *Day 3 Wed, September 28, 2016*, Dubai, UAE: SPE, Sep. 2016, p. D031S054R006. doi: 10.2118/181351-MS.
[49] B. Niu, A. Al-Menhali, and S. C. Krevor, 'The impact of reservoir conditions on the residual trapping of carbon dioxide in B erea sandstone', *Water Resources Research*, vol. 51, no. 4, pp. 2009–2029, Apr. 2015, doi: 10.1002/2014WR016441.
[50] A. Baban, A. Al-Yaseri, A. Keshavarz, R. Amin, and S. Iglauer, 'CO2 – brine – sandstone wettability evaluation at reservoir conditions via Nuclear Magnetic Resonance measurements', *International Journal of Greenhouse Gas Control*, vol. 111, p. 103435, Oct. 2021, doi: 10.1016/j.ijggc.2021.103435.
[51] VINCI Technologies, Inc., 'Relative Permeameter System - RPS700 - Operating Manual'. VINCI Technologies, Inc., 2014.
[52] C. Abou Mrad, F. Verga, and A. Suriano, 'Best practices for preparation of samples for laboratory analysis', Politecnico di torino, 2023.
[53] National Instutute os Standards and Technology, 'NIST Chemistry WevBook'. [Online]. Available: https://webbook.nist.gov/chemistry/fluid/
[54] D. N. Espinoza and J. C. Santamarina, 'Water-CO2-mineral systems: Interfacial tension, contact angle, and diffusion—Implications to CO2 geological storage', *Water Resources Research*, vol. 46, no. 7, Jul. 2010, doi: 10.1029/2009WR008634.
[55] X. Li, E. Boek, G. C. Maitland, and J. P. M. Trusler, 'Interfacial Tension of (Brines + CO_2): (0.864 NaCl + 0.136 KCl) at Temperatures between (298 and 448) K, Pressures between (2 and 50) MPa, and Total Molalities of (1 to 5) mol·kg^{-1}', *J. Chem. Eng. Data*, vol. 57, no. 4, pp. 1078–1088, Apr. 2012, doi: 10.1021/je201062r.
[56] M. Shiga, T. Morishita, and M. Sorai, 'Interfacial tension of carbon dioxide - water under conditions of CO2 geological storage and enhanced geothermal systems: A molecular dynamics study on the effect of temperature', *Fuel*, vol. 337, p. 127219, Apr. 2023, doi: 10.1016/j.fuel.2022.127219.